EE

KEK Preprint 96-141
TMU-HEP/EXP 96-10
November 1996
H

Polarimeter with Laser–Compton Scattering for Future Linear Colliders

H. Ishiyama[1], T. Hirose[1], T. Kumita[1],
Y. Kurihara[2], T. Okugi[1], T. Omori[2]

[1]*Department of physics, Tokyo Metropolitan University, Hachioji, Tokyo 192–03, Japan*
[2]*National Laboratory for High Energy Physics, (KEK), Tsukuba, Ibaraki 305, Japan*

CERN LIBRARIES, GENEVA
SCAN-9702055

Sw9708

Abstract

The transverse polarizations of beams in future e^+e^- linear colliders will provide an important tool for investigating e^+e^- physics. On the basis of laser-Compton scattering we propose to a new method to measure not only the longitudinal, but also the transverse, polarization near to the e^+e^- interaction point. This new polarimetry is based on asymmetry measurements of the angular distributions of scattered gamma–ray's for right– and left–handed laser beams. Since strong focussing of linear colliders at the interaction point results in a large angular spread of Compton–scattered gamma–ray's, the resolution of asymmetry measurements is highly deteriorated. The essential aspect of our polarimetry is to incorporate before the laser–$e^{\pm}$ collision point a quadrupole magnet which can focus $e^{\pm}$ beams with a spot size of 20 μm somewhere downstream, thus enabling us to determine the polarization vector with high precision. We propose a possible prescription to reject a huge amount of synchrotron radiation emerging in the process where the $e^{\pm}$ beams after a laser–$e^{\pm}$ collision are swept away through a bending magnet.

National Laboratory for High Energy Physics, 1996

KEK Reports are available from:

Technical Information & Library
National Laboratory for High Energy Physics
1-1 Oho, Tsukuba-shi
Ibaraki-ken, 305
JAPAN

Phone: 0298-64-5136
Telex: 3652-534 (Domestic)
(0)3652-534 (International)
Fax: 0298-64-4604
Cable: KEK OHO
E-mail: Library@kekvax.kek.jp (Internet Address)
Internet: http://www.kek.jp

1 Introduction

It is well known that the longitudinal polarizations of colliding electron(e^-)-positron(e^+) beams are very useful for detailed studies of electroweak theory. Transverse polarizations are also important for probing non-standard couplings of an e^-, and thus provide an interesting possibility to measure the relative phase of the helicity amplitudes [1], [2]. Since, in practice, beams are polarized partially longitudinal and partially transverse, a transversely polarized state is a superposition of the two helicity states with equal weight. Leptonic chiral symmetry implies that the transversely polarized cross section averaged over the azimuthal angle is equal to the total unpolarized cross section. Any deviation from this rule is a clear signal of " new physics " which breaks the leptonic chiral symmetry. Actually, we are systematically working to create polarized e^+ for future linear colliders [5]. For experiments with polarized beams, an accurate monitor of the beam polarization is essential, because the systematic uncertainty of the experiments highly depends on the accuracy of determining the polarization [4].

In a first-order approximation, the polarization of an $e^\pm$ beam at the injection point can be almost maintained and manipulated during its travel to the interaction point (IP) in a linear collider. This is the reason why the linear collider with highly polarized $e^\pm$ beams is a powerfull tool for performing experiments in which the initial state has a specific spin-state. In an actual linear collider, however, there will be various effects which cause depolarization of the $e^\pm$ beam. For example, the following components in a linear collider may affect the polarization: dipole and quadrupole magnets in the dumping ring, quadrupole magnets in the main linac and the final focus system, and spin rotators located at the upstreem and downstreem positions from the dumping ring. The interaction between the e^- and e^+ beams at the IP may also cause depolarization of the e^- and e^+ beams. Therefore, it is required to measure the polarization of the beams near to the IP. It is also important to estimate the true value of polarization at the IP, since a few to several percent of depolarization caused by the beam-beam effect is expected. A beam polarization monitor using laser-Compton scattering is suitable for this purpose, because no target material is required near to the IP.

Laser-Compton scattering to measure the beam polarization has been utilized for both circular accelarators and the SLC linear collider [8]. The SLC polarimeter is based on an asymmetry measurement of the energy distributions of scattered e^-'s by right- and left-handed circularly polarized laser beams[6]. However, this method can only measure the longitudinal polarization. In this report we present a new idea which is applicable for measuring both the longitudinal and the transverse polarization. The polarimeter is based on the asymmetry of the angular distribution of the scattered photon(γ)'s or $e^\pm$'s for the right- and left-handed circularly polarized laser beams.

In Sec 2 we present the kinematics and cross sections of the Compton scattering. The fundamental consideration on the Compton polarimeter is given in Sec 3. In particular, we discuss the technical details of measuring the transverse polarization, and present a new idea in Sec 4. The application of this polarimeter for JLC is considered in Sec 5.

2 Fomulation of Compton scattering

2.1 Kinematics of Compton scattering

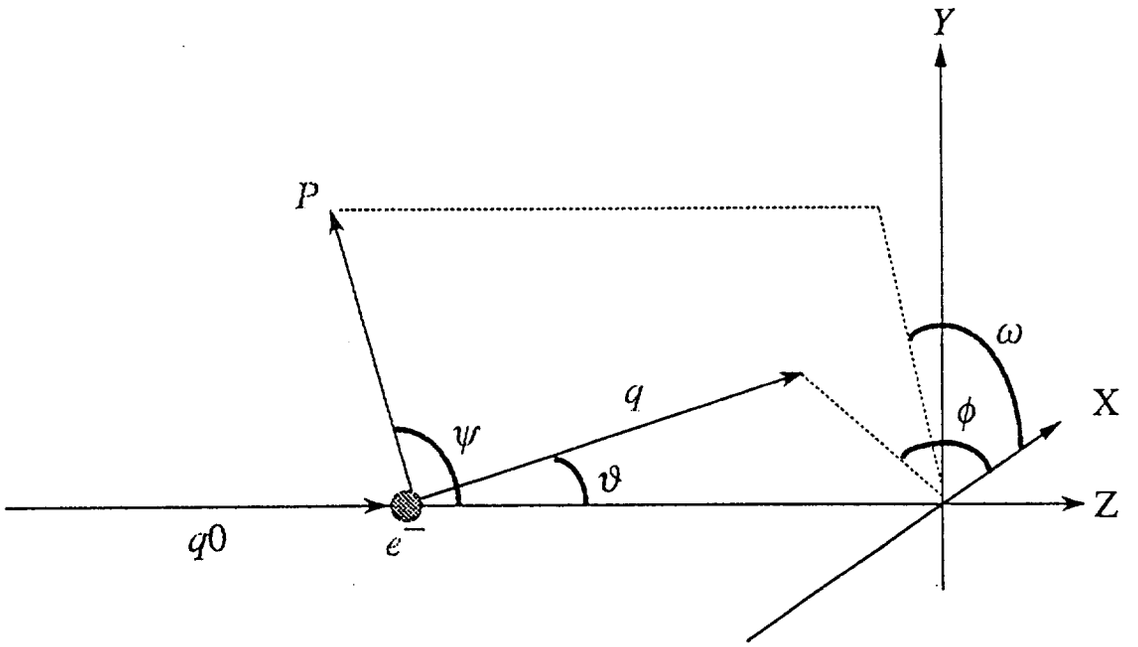

Figure 1: Electron rest system

We first consider the kinematics of Compton scattering in the electron rest system (Fig 1). The Z-axis is chosen to be along the direction of incoming γ's. The scattering angle (θ) is calculated by the following equation:

$$1 - \cos\theta = \frac{1}{q} - \frac{1}{q_0} , \tag{2.1}$$

where q_0 and q are the initial and final energies of the γ in units of the e^- rest mass (gamma factor). As shown in Fig 2, we choose the X_L-, Y_L-, and Z_L-axes in the laboratory system to be parallel to the X-, Y-, and Z-axes in the electron rest system. Assuming that the e^-'s are highly relativistic, ($\gamma_0 \gg 1$), and interact with a laser beam at a very small crossing angle ($\delta \ll 1$), the kinematics in the laboratory system can be rewritten as

$$2\gamma_0 k_0 \approx k(\gamma_0 + k_0) - k(\gamma_0 - k_0)\cos\theta_L , \tag{2.2}$$

where γ_0 is the gamma factor of the incident e^- beam, k_0 and k are those of the incident and scattered γ's in the laboratory system, and θ_L is the scattering angle of the γ. The

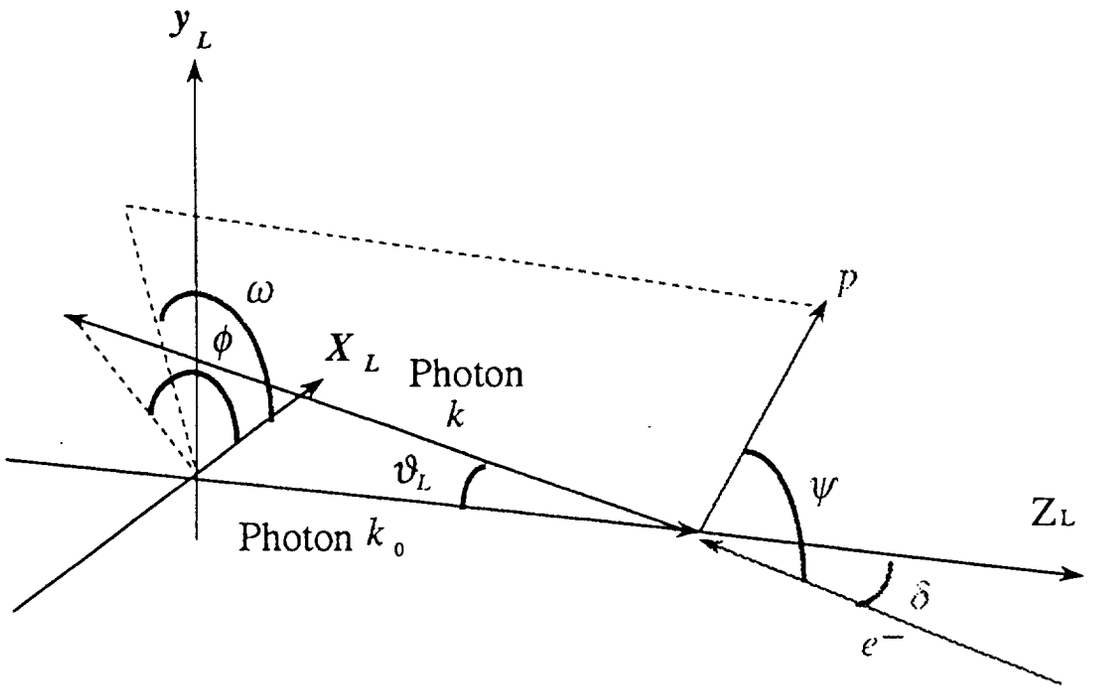

Figure 2: Laboratory system

scattered γ's are collimated backward in a small cone with respect to the opposite direction of the incident γ's. By applying the Lorentz transformation from the electron rest system to the laboratory system, the gamma factors and scattered angles are calculated by using

$$q_0 \approx 2\gamma_0 k_0 \ , \tag{2.3}$$

$$\tan\theta_L \approx \frac{\sin\theta}{\gamma_0(1-\cos\theta)} \ . \tag{2.4}$$

Furthermore, since a four-vector is invariant under a Lorentz transformation, the following relation is derived:

$$kk_0(1+\cos\theta_L) \approx qq_0(1-\cos\theta) = q_0 - q \ . \tag{2.5}$$

From Eq 2.1 $\sim$ Eq 2.5, θ is calculated as

$$\cos\theta \approx \frac{(2{\gamma_0}^2+1)k_0 - (2\gamma_0 k_0+1)k}{2\gamma_0 k_0(\gamma_0 - k)} \ . \tag{2.6}$$

Hence, the maximum and minimum energy of the scattered γ's and e^-'s are calculated as follows:

$$\begin{cases} k_{min} = k_0 \\ \gamma_{max} = \gamma_0 \end{cases} \qquad (for\ \theta = 0) \tag{2.7}$$

and

$$\begin{cases} k_{max} = \dfrac{k_0(4{\gamma_0}^2+1)}{4\gamma_0 k_0 + 1} \\ \\ \gamma_{min} = \dfrac{\gamma_0(4{k_0}^2+1)}{4\gamma_0 k_0 + 1} \end{cases} \qquad (for\ \theta = \pi)\ . \tag{2.8}$$

2.2 Cross sections of Compton scattering

In the electron rest system (Fig 1), the differential cross section of the Compton scattering is given as [3]

$$\frac{d\sigma}{d\Omega} = \frac{{r_e}^2}{2}\left(\frac{q}{q_0}\right)^2 [\,1 + \cos^2\theta + (q_0 - q)(1-\cos\theta) + \xi_1 \sin^2\theta \\ -\xi_3(1-\cos\theta)(\boldsymbol{q_0}\cos\theta + \boldsymbol{q})\cdot\boldsymbol{P}\,]\ , \tag{2.9}$$

where $r_e = e^2/mc^2$ is the classical e^- radius, $\boldsymbol{q_0}$ and $\boldsymbol{q}$ are the incident and scattered γ momenta, $\xi_1 = +1$ refers to the linear polarization of γ perpendicular to the the scattering plane, $\xi_3 = +1$ refers to the right-handed circular polarization of γ, and $\boldsymbol{P}$ is the polarization vector of the initial e^-. The polarization vector of the e^- spin can be specified in terms of polar coordinates (ψ, ω) :

$$P_x = P_e \sin\psi\cos\omega, \quad P_y = P_e \sin\psi\cos\omega, \quad P_z = P_e\cos\psi, \tag{2.10}$$

where P_e represents the magnitude of the e^- spin polarization. The momenta of the initial and scattered γ's are as follows:

$$q_{0x} = 0, \quad q_{0y} = 0, \quad q_{0z} = q_0, \tag{2.11}$$

$$q_x = q\sin\theta\cos\phi, \quad q_y = q\sin\theta\sin\phi, \quad q_z = q\cos\theta. \tag{2.12}$$

In general, the polarization of the γ's is specified by the Stokes parameters in the coordinate system, such that a polarization vector for $\xi_1 = +1$ refers to the positive direction perpendicular to the plane of scattering:

$$\begin{cases} \xi_1 = P_\gamma \cos 2\beta \cos 2(\phi - \alpha) \\ \xi_2 = -P_\gamma \cos 2\beta \sin 2(\phi - \alpha) \\ \xi_3 = P_\gamma \sin 2\beta\ , \end{cases} \tag{2.13}$$

where P_γ is the magnitude of the γ polarization, ϕ is the azimuthal angle of the scattering plane, and angles α and β determine the polarization ellipse describing the polarization

of the laser beam. From Eq 2.1 $\sim$ Eq 2.5, in the laboratory system (Fig 2), the cross section can be written as

$$\frac{d^2\sigma}{d\phi d\kappa} = \frac{d^2\sigma_0}{d\phi d\kappa} + \xi_1 \frac{d^2\sigma_1}{d\phi d\kappa} + \xi_3 \left[(P_x \sin\phi - P_y \cos\phi) \frac{d^2\sigma_2}{d\phi d\kappa} - P_z \frac{d^2\sigma_3}{d\phi d\kappa} \right] , \tag{2.14}$$

where κ is defined by the ratio of the scattered γ energy to its maximum possible energy, $\kappa \equiv k/k_{max}$. The differential cross sections are difined using the parameter

$$a = \frac{1}{(1 + 4\gamma_0 k_0)} \tag{2.15}$$

as

$$\frac{d^2\sigma_0}{d\phi d\kappa} = a{r_e}^2 \left\{ 1 + \frac{\kappa^2(1-a)^2}{1-\kappa(1-a)} + \left[\frac{1-\kappa(1+a)}{1-\kappa(1-a)} \right]^2 \right\} , \tag{2.16}$$

$$\frac{d^2\sigma_1}{d\phi d\kappa} = a{r_e}^2 \frac{4a\kappa(1-\kappa)}{[1-\kappa(1-a)]^2} , \tag{2.17}$$

$$\frac{d^2\sigma_2}{d\phi d\kappa} = a{r_e}^2 \frac{2(1-a)\kappa\sqrt{a\kappa(1-\kappa)}}{1-\kappa(1-a)} , \tag{2.18}$$

$$\frac{d^2\sigma_3}{d\phi d\kappa} = a{r_e}^2 [1-\kappa(1+a)] \left\{ 1 - \frac{1}{[1-\kappa(1-a)]^2} \right\} . \tag{2.19}$$

The scattering angle of γ in the laboratory system is given by

$$\tan\theta_L = \frac{1}{\gamma_0} \sqrt{\frac{1-\kappa}{\kappa a}} . \tag{2.20}$$

From Eq 2.14, it is found that the transverse component of the e^- polarization can be deduced by measuring the azimuthal angular distribution of scattered γ's due to the Compton scattering of a circularly polarized laser beam, and the longitudinal component can be obtained from their energy distribution.

We introduce the parameter κ_e, which is defined as the ratio of the scattered e^-'s energy to its possible maximum energy, $\kappa_e \equiv \gamma/\gamma_{max} = \gamma/\gamma_0$. From Eq 2.8 and $\gamma_0 + k_0 = \gamma + k$, κ_e is calculated to be

$$\kappa_e = 1 + \kappa(a-1) . \tag{2.21}$$

Using this relation, Eq 2.14 may be rewritten as

$$\begin{aligned} \frac{d^2\sigma}{d\phi_e d\kappa_e} &= \frac{d^2\sigma_0}{d\phi_e d\kappa_e} + \xi_1 \frac{d^2\sigma_1}{d\phi_e d\kappa_e} \\ &\quad + \xi_3 \left[(-P_x \sin\phi_e + P_y \cos\phi_e) \frac{d^2\sigma_2}{d\phi_e d\kappa_e} - P_z \frac{d^2\sigma_3}{d\phi_e d\kappa_e} \right] , \end{aligned} \tag{2.22}$$

where ϕ_e is the azimuthal angle of a scattered e^- in the laboratory system (difined by Fig 2). The corresponding differential cross sections are given as follows:

$$\frac{d^2\sigma_0}{d\phi_e d\kappa_e} = ar_e{}^2\left\{1+\frac{(1-\kappa_e)^2}{\kappa_e}+\left[\frac{(1+a)\kappa_e-2a}{\kappa_e(1-a)}\right]^2\right\}, \tag{2.23}$$

$$\frac{d^2\sigma_1}{d\phi_e d\kappa_e} = ar_e{}^2\frac{4(1-\kappa_e)(\kappa_e-a)}{[(1-a)\kappa_e]^2}, \tag{2.24}$$

$$\frac{d^2\sigma_2}{d\phi_e d\kappa_e} = ar_e{}^2\frac{2(1-\kappa_e)}{(1-a)\kappa_e}\sqrt{a(1-\kappa_e)(\kappa_e-a)}, \tag{2.25}$$

$$\frac{d^2\sigma_3}{d\phi_e d\kappa_e} = ar_e{}^2\frac{1}{1-a}[(1+a)\kappa_e-2a]\left(1-\frac{1}{\kappa_e{}^2}\right). \tag{2.26}$$

The scattering angle of e^- in the laboratory system is represented as

$$\tan\varphi_L = \frac{1-\kappa_e}{\gamma_0\kappa_e}\sqrt{\frac{\kappa_e-a}{a(1-\kappa_e)}}. \tag{2.27}$$

Eq 2.22 similarly reveals that the transverse(longitudinal) component of the e^- polarization can be obtained from a measurement of the azimuthal-angle (the energy) distributions of the scattered e^-'s.

3 Compton Polarimeter

3.1 Measurement of the polarization

Assuming that the amplitude of the betatron motion is a Gaussian distribution in the phase space of the e^- beam trajectory, the angular distribution of the scattered γ's projected on a detector placed at distance L downstream from the laser-e^- collision point (CP) is expressed as

$$\frac{d^2\sigma}{dXdY} = \int_\kappa^1 d\kappa\int_0^{2\pi} d\phi\, G_X(X+L\tan\theta_L\cos\phi)\, G_Y(Y+L\tan\theta_L\sin\phi)\frac{d^2\sigma}{d\phi d\kappa}. \tag{3.1}$$

The Gaussian-distribution function on the detector plane is given by

$$G_X(X) = \frac{1}{\sqrt{2\pi}\sigma_X}\,exp\left(-\frac{X^2}{2\sigma_X{}^2}\right), \quad \text{with} \quad \sigma_X = \sqrt{\varepsilon_x(\beta_x-2\alpha_x L+\gamma_x L^2)}, \tag{3.2}$$

where ε_x represents the horizontal emittance of the e^- beam, and $\alpha_x, \beta_x, \gamma_x$ are the Twiss parameters describing the horizontal phase space of the beam motion. The Gaussian-distribution function is nomalized as

$$\int_{-\infty}^{\infty} G_X(X)dX = 1. \tag{3.3}$$

Then, the horizontal distribution projected on the horizontal axis (X-axis) is obtained by

$$\begin{aligned}\frac{d\sigma}{dX}(X) &= \int_{-\infty}^{\infty} dY \frac{d^2\sigma}{dX\,dY} \\ &= \frac{1}{\sqrt{2\pi}\sigma_X}\int_{\kappa}^{1} d\kappa \int_0^{2\pi} d\phi\, exp\left[-\frac{(X + L\tan\theta_L\cos\phi)^2}{2{\sigma_X}^2}\right]\frac{d^2\sigma}{d\phi d\kappa}\,, \end{aligned} \tag{3.4}$$

where κ_c is the lower cut-off energy for γ detection. Similarly, the vertical distribution can be obtained by

$$\frac{d\sigma}{dY}(Y) = \frac{1}{\sqrt{2\pi}\sigma_Y}\int_{\kappa}^{1} d\kappa \int_0^{2\pi} d\phi\, exp\left[-\frac{(Y + L\tan\theta_L\sin\phi)^2}{2{\sigma_Y}^2}\right]\frac{d^2\sigma}{d\phi d\kappa}\,. \tag{3.5}$$

The distributions for the scattered e^-'s can be obtained by replacing κ with κ_e, ϕ with ϕ_e, and θ_L with φ_L.

Substituting Eq 2.14 into Eqs 3.4 and 3.5, and integrating over the azimuthal angle, we obtains the horizontal and vertical distribution functions as

$$\frac{d\sigma}{dX} = \frac{d\sigma_0}{dX} + S_1\frac{d\sigma_1}{dX} - S_3\left[P_x\frac{d\sigma_{2x}}{dX} + P_z\frac{d\sigma_3}{dX}\right] \tag{3.6}$$

and

$$\frac{d\sigma}{dY} = \frac{d\sigma_0}{dY} + S_1\frac{d\sigma_1}{dY} - S_3\left[P_y\frac{d\sigma_{2y}}{dY} + P_z\frac{d\sigma_3}{dY}\right]\,, \tag{3.7}$$

where S_1, S_2, S_3 are the Stokes parameters, defined as

$$\begin{cases} S_1 = P_\gamma\cos 2\beta\cos 2\alpha \\ S_2 = P_\gamma\cos 2\beta\sin 2\alpha \\ S_3 = P_\gamma\sin 2\beta\,, \end{cases} \tag{3.8}$$

and $d\sigma_i/dX$ $(i = 0 \sim 3)$ are explicitly expressed as below; the horizontal distribution functions are:

$$\begin{aligned}\frac{d\sigma_0}{dX}(X) &= \frac{1}{\sqrt{2\pi}\sigma_X}\int_{\kappa}^{1} d\kappa \int_0^{2\pi} d\phi\, exp\left[-\frac{(X + L\tan\theta_L\cos\phi)^2}{2{\sigma_X}^2}\right]\frac{d^2\sigma_0}{d\phi d\kappa}\,, \\ \frac{d\sigma_1}{dX}(X) &= \frac{1}{\sqrt{2\pi}\sigma_X}\int_{\kappa}^{1} d\kappa \int_0^{2\pi} d\phi\, exp\left[-\frac{(X + L\tan\theta_L\cos\phi)^2}{2{\sigma_X}^2}\right]\cos 2\phi\frac{d^2\sigma_1}{d\phi d\kappa}\,, \\ \frac{d\sigma_{2x}}{dX}(X) &= \frac{1}{\sqrt{2\pi}\sigma_X}\int_{\kappa}^{1} d\kappa \int_0^{2\pi} d\phi\, exp\left[-\frac{(X + L\tan\theta_L\cos\phi)^2}{2{\sigma_X}^2}\right]\sin\phi\frac{d^2\sigma_{2x}}{d\phi d\kappa}\,, \\ \frac{d\sigma_3}{dX}(X) &= \frac{1}{\sqrt{2\pi}\sigma_X}\int_{\kappa}^{1} d\kappa \int_0^{2\pi} d\phi\, exp\left[-\frac{(X + L\tan\theta_L\cos\phi)^2}{2{\sigma_X}^2}\right]\frac{d^2\sigma_3}{d\phi d\kappa}\,, \end{aligned}$$

and the vertical distribution functions are:

$$\frac{d\sigma_0}{dY}(Y) = \frac{1}{\sqrt{2\pi}\sigma_Y}\int_\kappa^1 d\kappa \int_0^{2\pi} d\phi\, exp\left[-\frac{(Y+L\tan\theta_L\sin\phi)^2}{2{\sigma_Y}^2}\right]\frac{d^2\sigma_0}{d\phi d\kappa}\ ,$$

$$\frac{d\sigma_1}{dY}(Y) = \frac{1}{\sqrt{2\pi}\sigma_Y}\int_\kappa^1 d\kappa \int_0^{2\pi} d\phi\, exp\left[-\frac{(Y+L\tan\theta_L\sin\phi)^2}{2{\sigma_Y}^2}\right]\cos 2\phi\frac{d^2\sigma_1}{d\phi d\kappa}\ ,$$

$$\frac{d\sigma_{2y}}{dY}(Y) = \frac{1}{\sqrt{2\pi}\sigma_Y}\int_\kappa^1 d\kappa \int_0^{2\pi} d\phi\, exp\left[-\frac{(Y+L\tan\theta_L\sin\phi)^2}{2{\sigma_Y}^2}\right]\cos\phi\frac{d^2\sigma_{2y}}{d\phi d\kappa}\ ,$$

$$\frac{d\sigma_3}{dY}(Y) = \frac{1}{\sqrt{2\pi}\sigma_Y}\int_\kappa^1 d\kappa \int_0^{2\pi} d\phi\, exp\left[-\frac{(Y+L\tan\theta_L\sin\phi)^2}{2{\sigma_Y}^2}\right]\frac{d^2\sigma_3}{d\phi d\kappa}\ ,$$

where parity of each distribution function is found to be

$$\frac{d\sigma_0}{dX}(-X) = \frac{d\sigma_0}{dX}(X)\ ,\ \frac{d\sigma_1}{dX}(-X) = \frac{d\sigma_1}{dX}(X)\ ,$$
$$\frac{d\sigma_2}{dX}(-X) = -\frac{d\sigma_2}{dX}(X)\ ,\ \frac{d\sigma_3}{dX}(-X) = \frac{d\sigma_3}{dX}(X)$$

and

$$\frac{d\sigma_0}{dY}(-Y) = \frac{d\sigma_0}{dY}(Y)\ ,\ \frac{d\sigma_1}{dY}(-Y) = \frac{d\sigma_1}{dY}(Y)\ ,$$
$$\frac{d\sigma_{2y}}{dY}(-Y) = -\frac{d\sigma_{2y}}{dY}(Y)\ ,\ \frac{d\sigma_3}{dY}(-Y) = \frac{d\sigma_3}{dY}(Y)\ .$$

Therefore, the Compton scattering of a circularly polarized laser beam by a transversely polarized e^- beam produces left-right asymmetry in the distribution of backscattered γ's or scattered e^-'s on the horizontal axis, and up-down asymmetry in the distribution on the vertical axis. The transverse components of the e^-–polarization vector can be definitely extracted from measurements of the horizontal and vertical distributions of the scattered γ's or e^-'s for the right–handed ($S_3 = +1$) and left–handed ($S_3 = -1$) circularly polarized laser beams. The longitudinal component of the e^- polarization is also obtained from measuring the transverse distribution of the γ's or e^-'s for two states of a circularly polarized laser beam. With an unpolarized e^- beam, one may determine the linear component (S_1) of the γ polarization. Typical patterns of horizontal and vertical distributions of scattered γ's and e^-'s at a downstream position from the IP are given under various conditions with $S_1 = 0$ ((a) $P_x = +1$, $S_3 = \pm 1$ (b) $P_y = +1$, $S_3 = \pm 1$ (c) $P_z = +1$, $S_3 = \pm 1$) in Figs 3 and 5. Here, we assume that the laser beam collided the e^- beam after the IP when the quadrupole magnets [QC1,QC2] (see Fig 14) used to focus the e^- beam are switched off. In this case, we attempted to optimize the detection resolution as a function of the distance between the QC2 magnet and the detector position, and found this distance to be 59 m. Table 1 lists the Twiss parameters at the QC2 magnet. The reason why the horizontal distributions are different from the vertical distributions is that the e^- beam for the JLC is very flat, i.e., the horizontal and vertical sizes at the

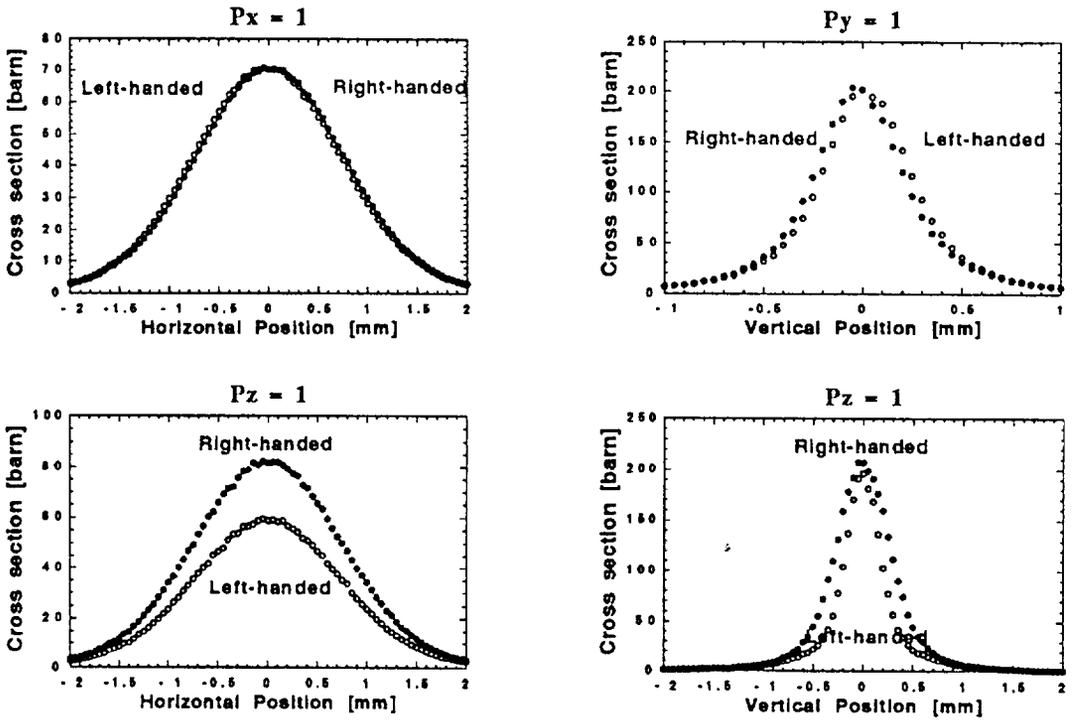

Figure 3: Distribution of the scattered γ's on a detector 59 m downstream from the QC2 magnet

CP are 659 μm and 121 μm, respectively. Thus, the transverse components of the e^- polarization vector can be calculated as

$$P_x = \frac{A_x}{S_3 \Pi_x} \quad \text{and} \quad P_y = \frac{A_y}{S_3 \Pi_y} \,, \tag{3.9}$$

where A_x and A_y are the left-right and up-down asymmetry, respectively, given by

$$A_x(X) = \frac{N_X(-,+) - N_X(+,+) - N_X(-,-) + N_X(+,-)}{N_X(-,+) + N_X(+,+) + N_X(-,-) + N_X(+,-)} \tag{3.10}$$

and

$$A_y(Y) = \frac{N_Y(-,+) - N_Y(+,+) - N_Y(-,-) + N_Y(+,-)}{N_Y(-,+) + N_Y(+,+) + N_Y(-,-) + N_Y(+,-)} \,. \tag{3.11}$$

Here, $N_X(a,b)$ represents the X–distributions of scattered γ or e^- for parameters a and b ; $a = +$ ($a = -$) means right–handed (left–handed) circularly polarized laser beam and $b = +$ ($b = -$) corresponds to the number of events in $X > 0$ ($X < 0$):

Table 1: Twiss parameters at the QC2 magnet

α_x	-246.08	α_y	-606.4
β_x	18550.7	β_y	35792.9
γ_x	3.26437	γ_y	10.27360

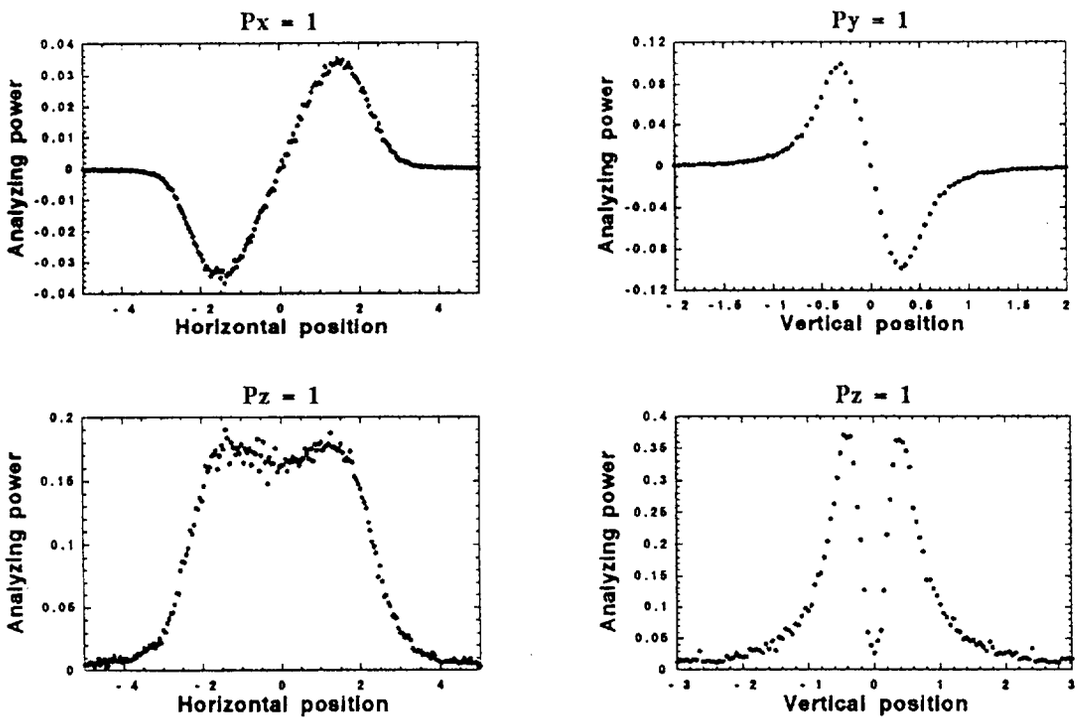

Figure 4: Analyzing power of the asymmetry measurement for γ on a detector 59 m downstream from the QC2 magnet

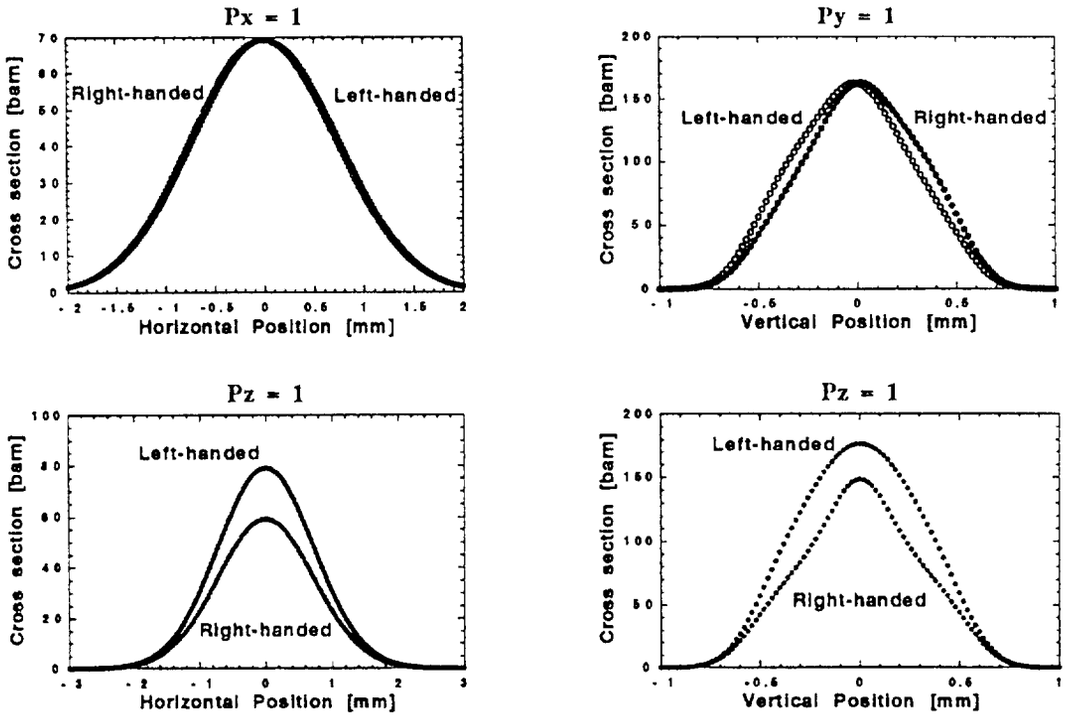

Figure 5: Distribution of scattered e^-'s on a detector 59 m downstream from the QC2 magnet

$$
\begin{aligned}
N_X(+,+) &= L_m \int_{X_1}^{X_2} dX \frac{d\sigma}{dX} \ , \ N_X(+,-) = L_m \int_{-X_2}^{-X_1} dX \frac{d\sigma}{dX} \quad (S_3 > 0) \ , \\
N_X(-,+) &= L_m \int_{X_1}^{X_2} dX \frac{d\sigma}{dX} \ , \ N_X(-,-) = L_m \int_{-X_2}^{-X_1} dX \frac{d\sigma}{dX} \quad (S_3 < 0) \ ,
\end{aligned}
$$

where L_m is the integrated luminosity of an e^- beam and a laser–beam interaction; $0 \leq X_1 \leq X_2$. $N_Y(\pm,\pm)$ represents the Y–distributions, and is defined as for $N_X(\pm,\pm)$ as

$$
\begin{aligned}
N_Y(+,+) &= L_m \int_{Y_1}^{Y_2} dY \frac{d\sigma}{dY} \ , \ N_Y(+,-) = L_m \int_{-Y_2}^{-Y_1} dY \frac{d\sigma}{dY} \quad (S_3 > 0) \ , \\
N_Y(-,+) &= L_m \int_{Y_1}^{Y_2} dY \frac{d\sigma}{dY} \ , \ N_Y(-,-) = L_m \int_{-Y_2}^{-Y_1} dY \frac{d\sigma}{dY} \quad (S_3 < 0) \ ,
\end{aligned}
$$

where $0 \leq Y_1 \leq Y_2$. Π_x and Π_y are the analyzing powers of a transverse polarization measurement, defined by the ratio of the spin-dependent term of the cross sections to the spin-independent term. They are calculated by integrating the cross–section coupling to

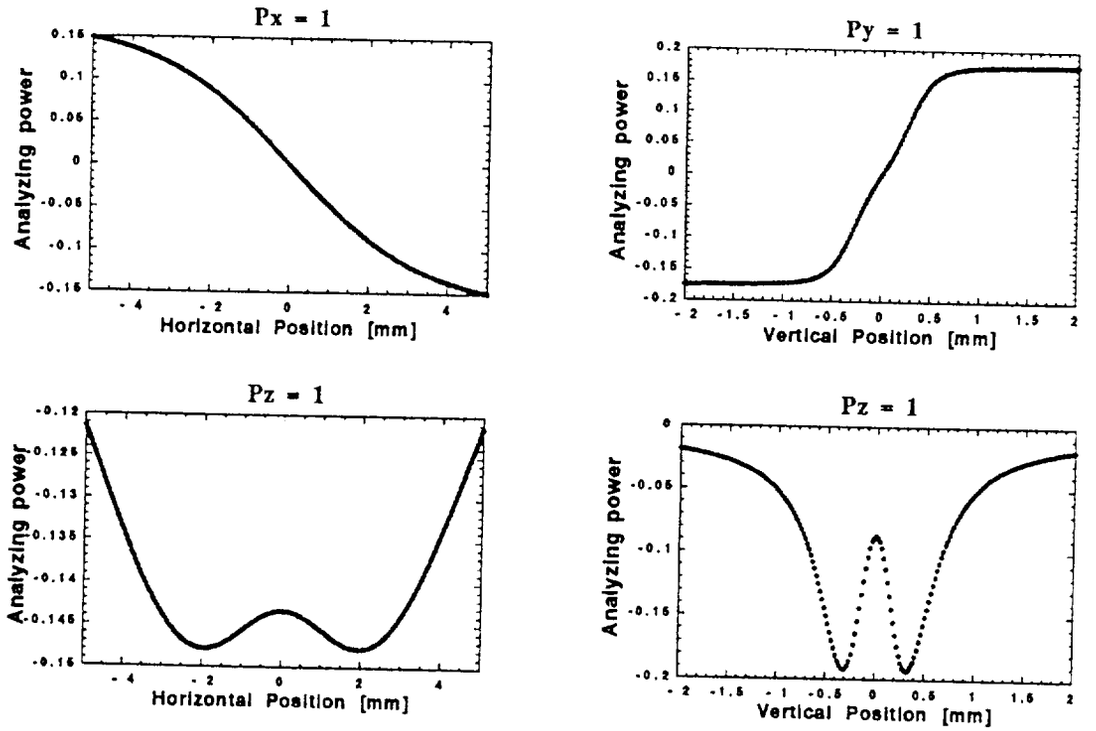

Figure 6: Analyzing power of the asymmetry measurement for e^- on a detector 59 m downstream from the QC2 magnet

each component of the polarization vector over the kinematic acceptance of the asymmetry measurement as

$$\Pi_x(X) = \frac{\sigma_{2x}(X_1 \leq X \leq X_2)}{\sigma_0(X_1 \leq X \leq X_2)} \quad and \quad \Pi_y(Y) = \frac{\sigma_{2y}(Y_1 \leq Y \leq Y_2)}{\sigma_0(Y_1 \leq Y \leq Y_2)} \ , \tag{3.12}$$

where

$$\begin{aligned} \sigma_0(X_1 \leq X \leq X_2) &= \int_{X_1}^{X_2} dX \frac{d\sigma_0}{dX} \ , \ \sigma_{2x}(X_1 \leq X \leq X_2) = \int_{X_1}^{X_2} dX \frac{d\sigma_{2x}}{dX} \ , \\ \sigma_0(Y_1 \leq Y \leq Y_2) &= \int_{Y_1}^{Y_2} dY \frac{d\sigma_0}{dY} \ , \ \sigma_{2y}(Y_1 \leq Y \leq Y_2) = \int_{Y_1}^{Y_2} dY \frac{d\sigma_{2y}}{dY} \ . \end{aligned}$$

Taking into account the definitions of asymmetry given by Eqs 3.10 and 3.11, the transverse polarization parameters can be determined by Eq 3.9, even in the more general case of an elliptically polarized laser beam. In these definitions, the terms coupling to the linear laser polarization and the longitudinal e^- polarization are cancelled out. For a

completely circular-polarized laser beam with $S_1 = 0$, the longitudinal component of the polarization vector can be extracted from

$$P_z = \frac{A_z}{S_3 \Pi_z} , \tag{3.13}$$

where the asymmetry is defined as

$$A_z(X) = \frac{N_X(+,+) + N_X(+,-) - N_X(-,+) - N_X(-,-)}{N_X(+,+) + N_X(+,-) + N_X(-,+) + N_X(-,-)} \tag{3.14}$$

and the analyzing power is

$$\Pi_z(X) = \frac{\sigma_3(X_1 \leq X \leq X_2)}{\sigma_0(X_1 \leq X \leq X_2)} . \tag{3.15}$$

The same expression can be obtained from the vertical distribution. The distribution of each analyzing power in transverse-polarization measurements is shown in Figs 4 and 6.

The longitudinal polarization is insensitive to the transverse distribution of scattered γ's (e^-'s), but is more sensitive to the energy distribution of these γ's (e^-'s). By integrating Eqs 2.14 and 2.22 over each azimuthal angle, only the spin-independent term and the cross-section coupling to the longitudinal polarization remain, respectively:

$$\frac{d\sigma}{d\kappa} = \int_0^{2\pi} d\phi \frac{d^2\sigma}{d\phi d\kappa} = \frac{d\sigma_0}{d\kappa} - S_3 P_z \frac{d\sigma_3}{d\kappa} , \tag{3.16}$$

$$\frac{d\sigma}{d\kappa_e} = \int_0^{2\pi} d\phi_e \frac{d^2\sigma}{d\phi_e d\kappa_e} = \frac{d\sigma_0}{d\kappa_e} - S_3 P_z \frac{d\sigma_3}{d\kappa_e} . \tag{3.17}$$

The energy distributions of the γ's and e^-'s for an e^--beam energy of 250 GeV and a laser energy of 2.33 eV are illustrated in Figs 7 and 8, respectivery, for $P_z = +1, S_3 = \pm 1$, and nonpolarization. Thus, the longitudinal polarization can be obtained by taking the difference between measurements with the left- and right-handed circularly polarized laser beams as

$$P_z = \frac{A_\kappa}{S_3 \Pi_z} , \tag{3.18}$$

where A_κ is the asymmetry in the energy distribution, defined as

$$A_\kappa = \frac{N_\kappa(+) - N_\kappa(-)}{N_\kappa(+) + N_\kappa(-)} . \tag{3.19}$$

Here, $N_\kappa(\pm)$ is the number of events counted by the calorimeter within given energy cuts,

$$N_\kappa(+) = L_m \int_{\kappa_1}^{\kappa_2} d\kappa \frac{d\sigma}{d\kappa} \quad (S_3 > 0) , \; N_\kappa(-) = L_m \int_{\kappa_1}^{\kappa_2} d\kappa \frac{d\sigma}{d\kappa} \quad (S_3 < 0) , \tag{3.20}$$

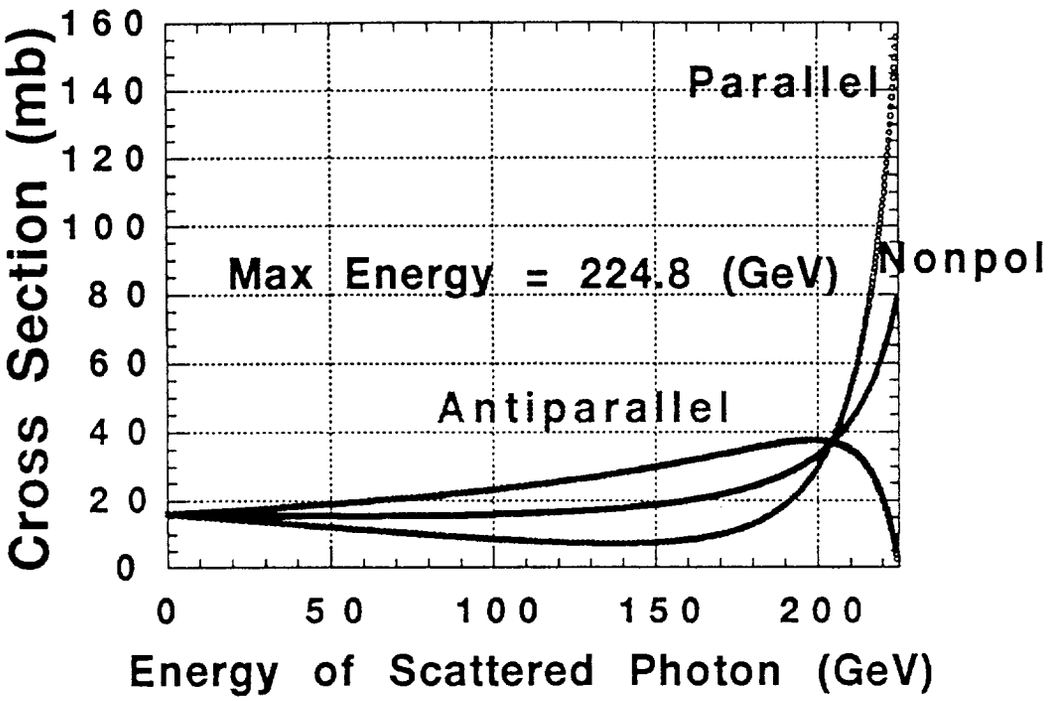

Figure 7: Energy distribution of the scattered γ's for an e^- beam of 250 GeV and a laser beam of 2.33 eV for JLC

where $0 \leq \kappa_1 \leq \kappa_2 \leq 1$. Π_z is the analyzing power of the longitudinal-polarization measurement, defined by

$$\Pi_z = \frac{\sigma_3(\kappa_1 \leq \kappa \leq \kappa_2)}{\sigma_0(\kappa_1 \leq \kappa \leq \kappa_2)} , \tag{3.21}$$

where the cross sections can be explicitly integrated as

$$\begin{aligned} \sigma_0(\kappa_1 \leq \kappa \leq \kappa_2) &= \int_{\kappa_1}^{\kappa_2} d\kappa \frac{d\sigma_0}{d\kappa} = 2\pi a r_e^2 \left\{ \left(\frac{1+a}{1-a}\right)^2 (\kappa_2 - \kappa_1) - \frac{1-a}{2}(\kappa_2^2 - \kappa_1^2) \right. \\ &\left. + \frac{3a^2+6a-1}{(1-a)^3} \ln \frac{\rho(\kappa_2)}{\rho(\kappa_1)} + \frac{4a^2}{(1-a)^3} \left[\frac{1}{\rho(\kappa_2)} - \frac{1}{\rho(\kappa_1)} \right] \right\}, \end{aligned} \tag{3.22}$$

$$\begin{aligned} \sigma_3(\kappa_1 \leq \kappa \leq \kappa_2) &= \int_{\kappa_1}^{\kappa_2} d\kappa \frac{d\sigma_3}{d\kappa} = 2\pi a r_e^2 \left\{ \kappa_2 - \kappa_1 - \frac{1+a}{2}(\kappa_2^2 - \kappa_1^2) \right. \\ &\left. + \frac{1+a}{(1-a)^2} \ln \frac{\rho(\kappa_2)}{\rho(\kappa_1)} + \frac{2a}{(1-a)^2} \left[\frac{1}{\rho(\kappa_2)} - \frac{1}{\rho(\kappa_1)} \right] \right\}' \end{aligned} \tag{3.23}$$

where $\rho(\kappa) = 1 - \kappa(1-a)$.

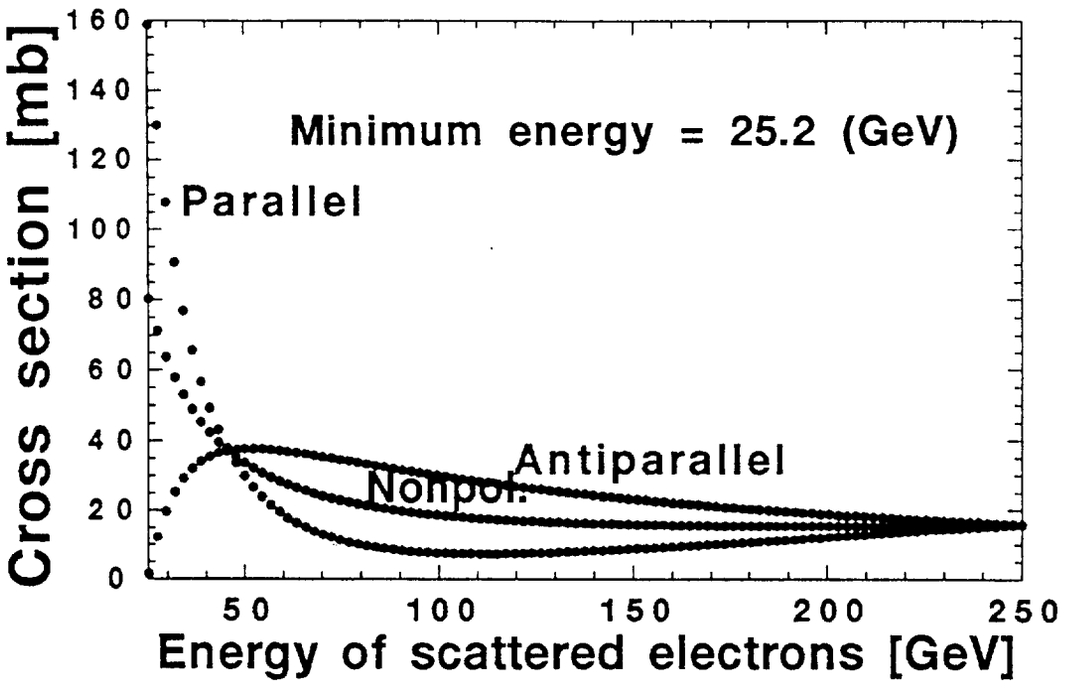

Figure 8: Energy distribution of scattered e^-'s for an e^- beam of 250 GeV and a laser beam of 2.33 eV for JLC

3.2 Considerations of the resolution

Each component of the e^- polarization vector (P_i $(i = x, y, z)$) is basically determined by the asymmetry of the Compton γ rates, the analyzing power (Π_i) and the γ polarization (S_3) as

$$P_i = \frac{1}{S_3 \Pi_i} \left(\frac{N(+) - N(-)}{N(+) + N(-)} \right) , \tag{3.24}$$

where $N(+)$ and $N(-)$ are the number of γ events counted by the detector for the two γ helicities with $S_3 > 0$ and $S_3 < 0$. The stastical accuracy of the polarization measurement is given by

$$\Delta P_i = \frac{2}{S_3 \Pi_i} \sqrt{\frac{N(+)N(-)}{\{N(+) + N(-)\}^3}} \sim \frac{1}{S_3 \Pi_i \sqrt{N}} , \tag{3.25}$$

where $N = N(+)+N(-)$. It is necessary not only to take a sufficient number of events, but to make a high analyzing power. Therefore, the relavant parameters of the polarization measurement should be chosen so as to optimize the quantity $\Pi^2 N \propto \Pi^2 \sigma_0$ in order to minimize the stastical error. The systematic error consists of uncertainties for measuring

the γ polarization and the analyzing power, *i.e.*

$$\frac{\Delta P_i}{P_i} = \left[\left(\frac{\Delta S_3}{S_3}\right)^2 + \left(\frac{\Delta \Pi_i}{\Pi_i}\right)^2\right]^{1/2} . \tag{3.26}$$

In order to analyze the degree of transverse polarization, the most likely range of the transverse position distribution over which the number of events is integrated is chosen so that the quantities ${\Pi_x}^2\sigma_0(X_1 \leq X \leq X_2)$ and ${\Pi_y}^2\sigma_0(Y_1 \leq Y \leq Y_2)$ are maximized. The maximum asymmetry of the scattered γ rate occurs at polar angles of $\theta \sim 1/\gamma$. The angular divergence of the beam and the angular resolution of the detector should be small compared to this angle so that the asymmetry of the distribution can be resolved. The net angular divergence of the beam on the detector is given by

$$\frac{\sigma_X}{L} = \sqrt{\left(\frac{\sigma_x}{\beta_x}\right)^2 \left[1 + \left(\alpha_x - \frac{\beta_x}{L}\right)^2\right] + \left(\frac{\sigma_D}{L}\right)^2} \tag{3.27}$$

and

$$\frac{\sigma_Y}{L} = \sqrt{\left(\frac{\sigma_y}{\beta_y}\right)^2 \left[1 + \left(\alpha_y - \frac{\beta_y}{L}\right)^2\right] + \left(\frac{\sigma_D}{L}\right)^2} , \tag{3.28}$$

where σ_x and σ_y are the horizontal and vertical beamsizes at the CP, and σ_D is the rms position resolution of the detector. The angular divergence should be minimized by making L as large as possible and by satisfying the condition, such that the quantity $(\alpha_x - \beta_x/L)^2$ or $(\alpha_y - \beta_y/L)^2$ is minimized. For example, the optimum location of the polarimeter for JLC may be determined from considerations on the vertical beam optics, since beams for JLC are very flat beam.

In order to analyze the degree of longitudinal polarization, we choose the most likely range of the longitudinal position distribution for scattered e^-'s over which the number of events is integrated so that the quantity ${\Pi_z}^2\sigma_0(\kappa_1 \leq \kappa \leq \kappa_2)$ is maximized. In measuring the energy κ with an error, the expectation value of the function $F(\kappa)$ is given by

$$< F >= \int_{-\infty}^{\infty} d\varepsilon P(\varepsilon, \kappa) F(\varepsilon) , \tag{3.29}$$

where $P(\varepsilon, \kappa)$ is the probability function, defined so that the probability that the value of a random measurement of the energy κ is found around κ, and is given by $\Delta k/k = C/\sqrt{k(GeV)}$, where the constant C is typically 0.05 in lead-glass calorimeters. Thus, the probability function is expressed by

$$P(\varepsilon, \kappa) = \frac{1}{\sqrt{2\pi\kappa}A} exp\left[-\frac{(\varepsilon - \kappa)^2}{2\kappa A^2}\right] , \tag{3.30}$$

where $A = C/\sqrt{k_{max}(GeV)}$. Taking into account the resolution of an energy measurement by using the calorimeter, the uncertainties in the cross sections are

$$\Delta\sigma_0(\kappa_1 \le \kappa \le \kappa_2) = 2\pi a r_e^2 A^2 \left\{ \frac{1-a}{2}(\kappa_1 - \kappa_2) + \frac{3a^2+6a-1}{2(1-a)} \left[\frac{\kappa_1}{\rho(\kappa_1)^2} - \frac{\kappa_2}{\rho(\kappa_2)^2} \right] + \frac{4a^2}{1-a} \left[\frac{\kappa_2}{\rho(\kappa_2)^3} - \frac{\kappa_1}{\rho(\kappa_1)^3} \right] \right\} , \quad (3.31)$$

$$\Delta\sigma_3(\kappa_1 \le \kappa \le \kappa_2) = 2\pi a r_e^2 A^2 \left\{ \frac{1+a}{2}(\kappa_1 - \kappa_2) + \frac{1+a}{2} \left[\frac{\kappa_1}{\rho(\kappa_1)^2} - \frac{\kappa_2}{\rho(\kappa_2)^2} \right] + 2a \left[\frac{\kappa_2}{\rho(\kappa_2)^3} - \frac{\kappa_1}{\rho(\kappa_1)^3} \right] \right\} . \quad (3.32)$$

Then, the uncertainty of the analyzing power is estimated to be

$$\frac{\Delta\Pi_z}{\Pi_z} = \sqrt{\left[\frac{\Delta\sigma_0(\kappa_1 \le \kappa \le \kappa_2)}{\sigma_0(\kappa_1 \le \kappa \le \kappa_2)} \right]^2 + \left[\frac{\Delta\sigma_3(\kappa_1 \le \kappa \le \kappa_2)}{\sigma_3(\kappa_1 \le \kappa \le \kappa_2)} \right]^2} , \quad (3.33)$$

where $\sigma_0(\kappa_1 \le \kappa \le \kappa_2)$ and $\sigma_3(\kappa_1 \le \kappa \le \kappa_2)$ are given by Eqs 3.22 and 3.23, respectively.

3.3 The Compton polarimeter for SLC

A Compton-scattering based polarimeter is used to measure the beam polarization near to the IP of e^+e^- at the SLAC Linear Collider (SLC) [8]. A schematic layout of the polarimeter is shown in Fig 9. The outgoing e^- beam is in the energy range of 45.7 GeV collides with a 2.33 eV circularly polarized laser beam at a point 33 m downstream from the IP. Since the Compton-scattering angle of the e^-'s is smaller than the angular divergence of the incident e^- beam, the scattered and unscattered e^-'s remain unseparated until they pass through a pair of SLC dipole magnets of field integral 3.05 T-m. The scattered e^-'s are dispersed horizontally, and exit the vacuum system through a thin window. The energy distribution of scattered e^-'s and analyzing power of the asymmetry measurement are illustrated in Figs 10 and 11, respectively. Then, the e^-'s in the energy range of 17–30 GeV are detected and their momenta are analyzed by a pair of multichannel detectors 3.57 m and 3.87 m downstream from effective bend center of the dipole pair. The differential cross section of the Compton scattering integrated over the azimuthal angle is given by Eq 3.17. The spin-independent and spin-dependent cross section functions are dependent on the energies of the e^- and laser beams. The cross section and asymmetry take maximum values at the kinematical limit of energy (17.4 GeV), corresponding to a scattering angle of 180 degrees in the electron rest system. The asymmetry is zero at an energy of 25.2 GeV, and becomes negative for larger energies. The counting rates in the detectors for two helicity states, $N_\kappa\ (S_3 = +1)$ and $N_\kappa\ (S_3 = -1)$, are measured ,respectively. It follows from Eq 3.19 that the asymmetry formed from these rates determines the longitudinal polarization of the e^- beam,

$$P_z = \frac{1}{S_3 \Pi_z} \left(\frac{N_\kappa(+) - N_\kappa(-)}{N_\kappa(+) + N_\kappa(-)} \right) . \quad (3.34)$$

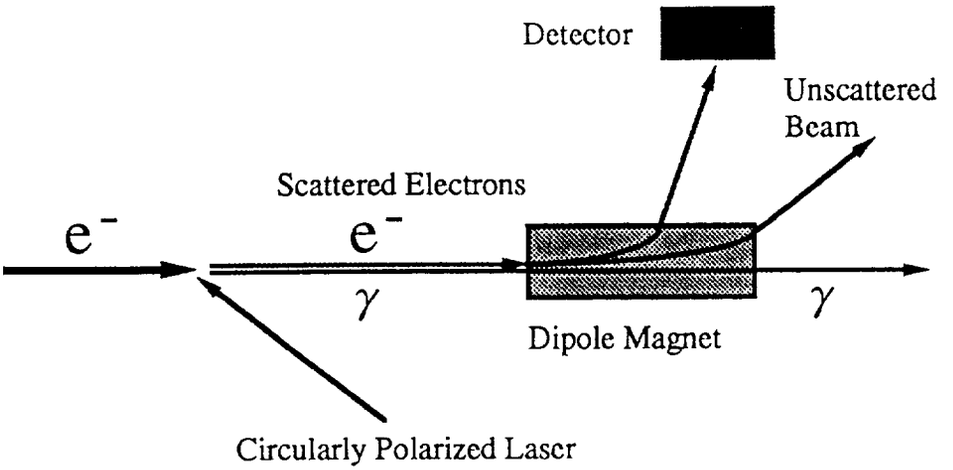

Figure 9: Schematic layout of the polarimeter for the SLC e^- beam

4 New method for polarimetry

4.1 JLC (Japan Linear Collider)

The most essential point in applying a Compton-scattering based polarimeter for future linear colliders is the choice of the laser-$e^{\pm}$ collision point (CP), because the analyzing power of asymmetry measurements is highly dependent on the profile of the e^- beam projected onto the detector. As discussed in Sec 1, the beam polarization should be measured near to the IP. It is obviously better to measure the polarization during e^+e^- collision experiments.

The JLC(Japan Linear Collider) project is one of the post-TRISTAN high-energy physics program in Japan. The project consists of constructing of a linear collider and experimental facilities therewith at an initial center of mass energy of around 500 GeV, which will eventually reach 1.5 TeV along with successive machine upgrades(1, 2, 3). The main purpose of JLC-I, with a center-of-mass energy range of up to 500 GeV with a peak luminosity of $5 \times 10^{33}\mathrm{cm}^{-2}\mathrm{sec}^{-1}$, is to discover the Higgs boson, to study the detailed nature of the top quark and to discover new phenomena beyond Standard Model. To achieve this aim with a reasonable total length of 25 to 30 km, the main linac may be operated in the X-band (11424MHz) frequency with multiple-bunch operation. Each bunch consists of about 2×10^{10} particles; the number of bunches per RF pulse is about 100. The recent demand of particle physics, however, puts more emphasis on a relatively low-energy range of $\sqrt{s}$ = 300 to 500 GeV, and on an earlier start of the experiment around the year 2000. If early construction is desired, it seems that the possibility of a frequency range lower than the X-band should also be pursued. Now, three frequencies, (S-

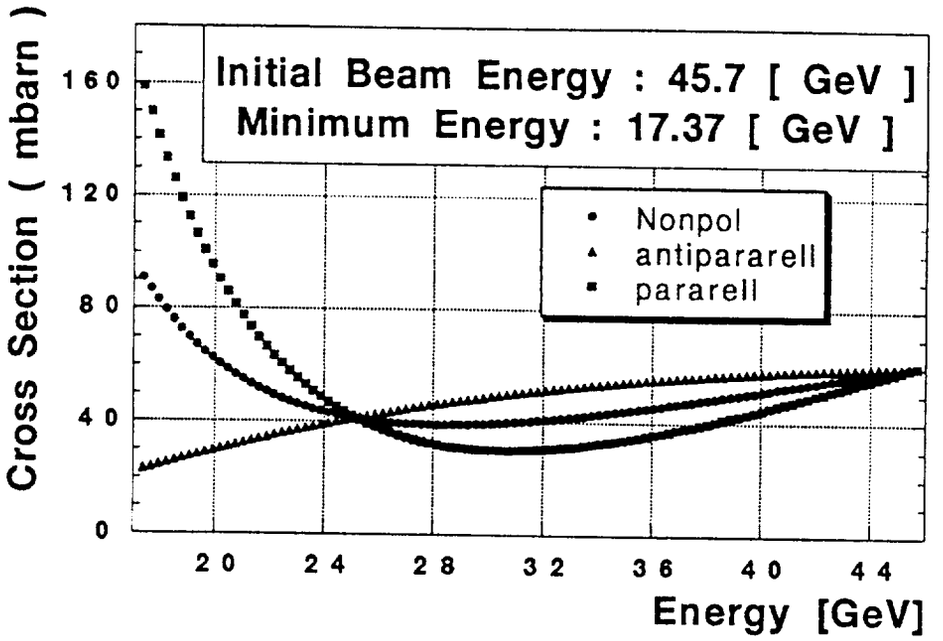

Figure 10: Energy distribution of scattered e^-'s for an e^- beam of 45.7 GeV and a laser beam of 2.33 eV for SLC

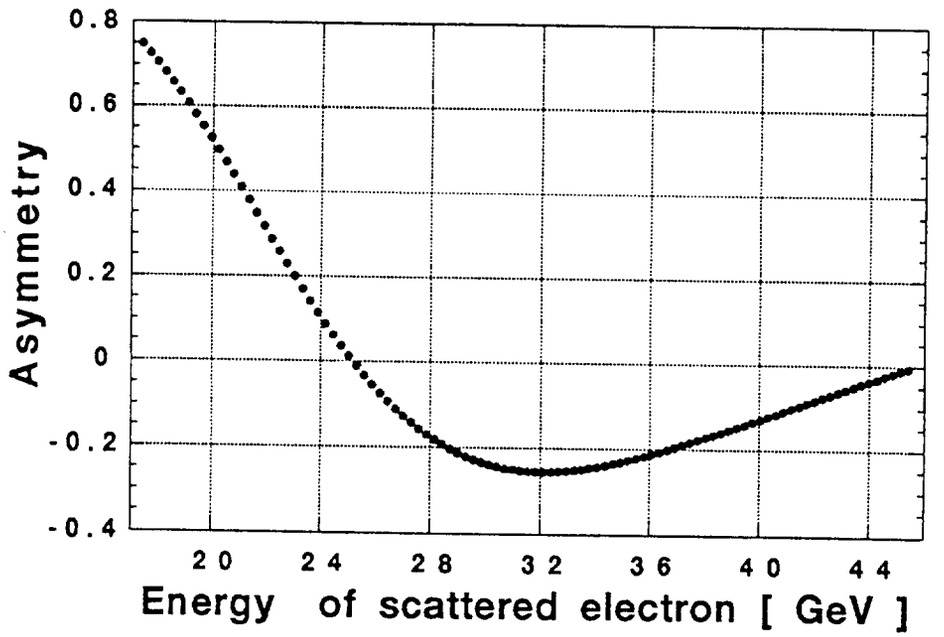

Figure 11: Analyzing power of the asymmetry measurement for scattered e^-'s for SLC

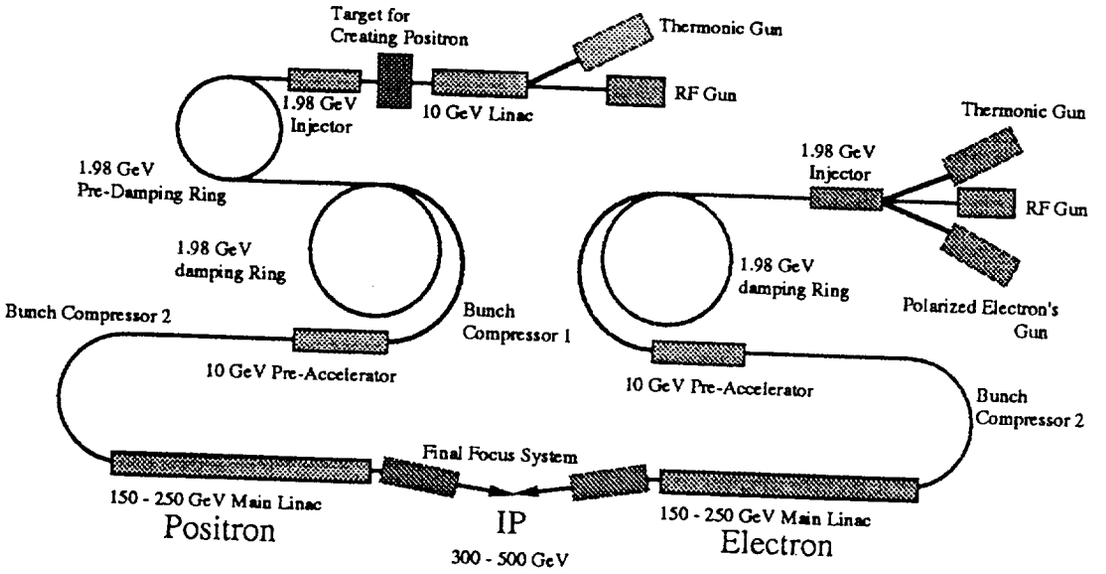

Figure 12: Schematic layout of JLC-I

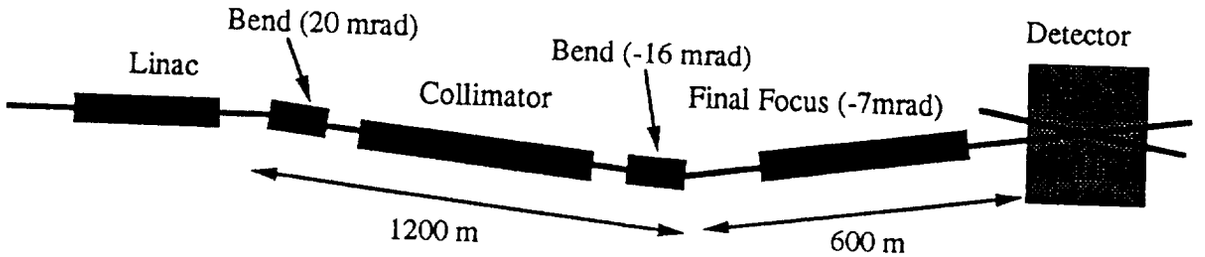

Figure 13: Schematic layout of the final focus system for JLC-I

band (2856MHz), C-band (5712MHz), and X-band) are being considered. The parameter set given here has not yet been fully studied. It is intended only to serve as a starting point of a design study. Fig 12 shows a schematic layout of JLC-I [5].

The characteristics of the final focus system is important for a Compton-scattering based polarimeter system. The final focus system for JLC consists of two parts: the first one is a focusing optical system, which provides the required nanometer beam profile at the IP; the second is a collimator section located between the linac and the focusing optics. Fig 13 shows a schematic layout of the entire final focus system [5], and Table 2 lists the main parameters of the final focus system of the beam in the energy range of 250 GeV. The length of the free area for the detector around the IP is set to be $l^* = 2.5$ m, which is sufficient to place the masks against background, to place beam-position monitors for the beam-beam steering, to make a side-hole at the final quadrupoles to let the beam escape after the collision, and to place a super-conducting shield of the quadrupoles for

Table 2: Parameters of the final focus system for JLC

Beam energy	E_0	250	GeV
Incoming invariant emittances	$\varepsilon_x/\varepsilon_y$	$3.6\times10^{-6}/5.0\times10^{-8}$	m·rad
Invariant emittances at IP	$\varepsilon_x/\varepsilon_y$	$3.8\times10^{-6}/6.0\times10^{-8}$	m·rad
β functions at the IP	β_x^*/β_y^*	10/0.1	mm
Spot sizes at the IP	σ_x^*/σ_y^*	280/3.5	nm
Free area length	l^*	2.5	m
Half aperture of the final quadrupole magnet	a	6.8	mm
Pole-tip field	B_0	1.3	T
Length of the final quadrupole magnet	L_1	2.2	m
Total bend angle	θ	7.1	mrad

Table 3: Twiss parameters at the IP

α_x^*	-0.03215	α_y^*	0.01271
β_x^*	0.00990	β_y^*	8.80×10^{-5}
γ_x^*	101.01	γ_y^*	11363.64

the solenoid field of the detector.

4.2 Achievement of higher resolution for the polarization measurement

Although in Sec 3.1 we considered polarization measurements by switching off the final focussing magnets (QC1, QC2), it might be better to measure the polarization without stoping data-taking. The polarization should be measured near to the IP during an e^+e^- collision experiment. The Twiss parameters at the IP are listed in Table 3. As discussed in Sec 3.2, we should make the distance between the CP and γ detector (L) as long as possible. If we select a position 1 m downstream from the IP as the CP, the analyzing power of the measurements cannot be sufficiently high, because the beam sizes downstream from the IP becomes large as a result of the strong beam focusing at the IP. Consequently, we can achieve only 2% of the analyzing powers for the transverse-polarization measurement. Since the $e^\pm$ beams of JLC cross each other at a very small angle of a few mrad, the one outgoing beam, e.g. e^-, passes through the off-center region of the quadrupole magnets (QC2,QC1), which focus another beam, e.g. e^+. The quick expansion of the beamsize after the IP deteriorates the accuracy of the polarization measurement. Since the magnetic field of QC1 is about 0.5 T, even at the off-center region of the magnet, the trajectory of the outgoing e^- beam is bent, as shown in Fig 14.

Therefore, we need to refocus the beam so as to be as small as possible at a downstream

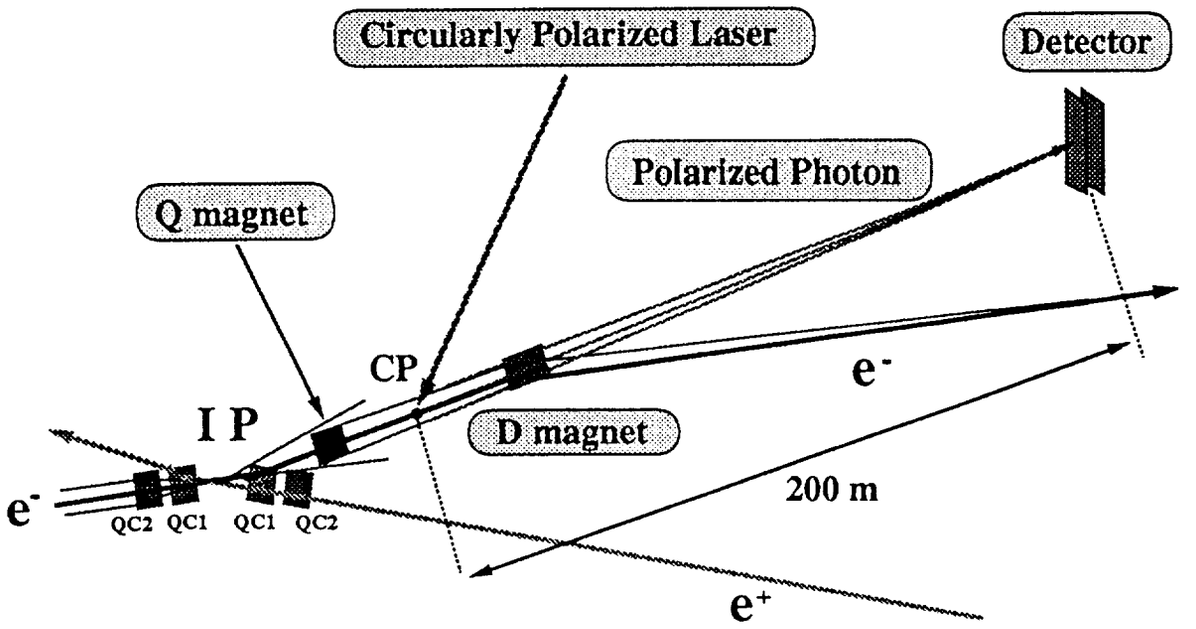

Figure 14: Proposed layout of the polarimeter for JLC

point with a distance L from the CP. Accordingly, we locate other quadrupole magnets at a downstream position from QC1, as shown in Fig 14. Assuming that L is set to be 200 m, the e^- beam projected on the detector is able to focus down to 20 μm, which is possible using today's technologies. Convoluting the finite size (20 μm) of the $e^{\pm}$ beams, we calculate the angular distributions of scattered γ's(e^-'s) on the detector plane, as shown in Fig 4.2(4.2), and the analyzing powers of an asymmetry measurement, as shown in Fig 4.2(4.2). Thus, we can obtain over 10% of the analyzing power for measuring the transverse polarization during e^+e^- collision experiments.

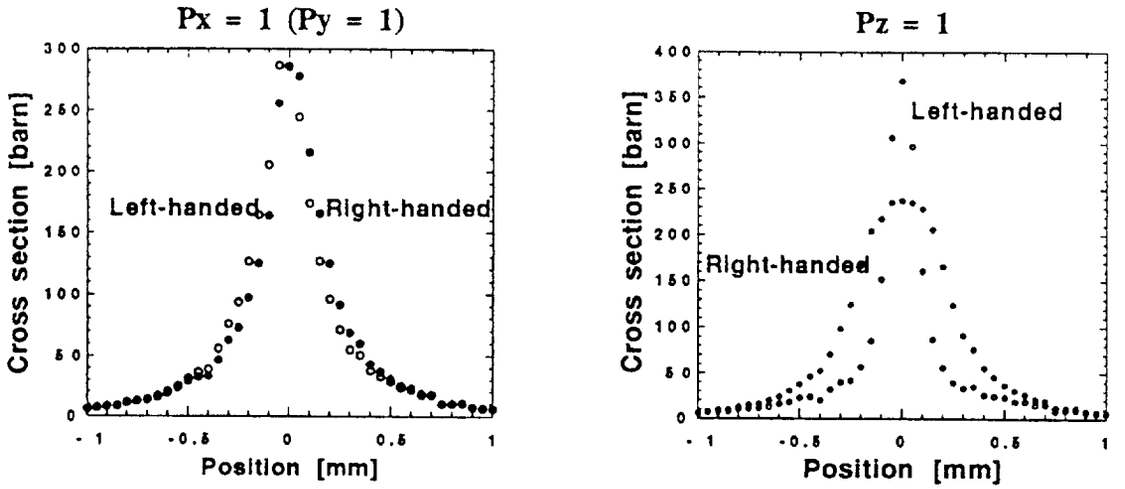

Figure 15: Distribution of scattered γ's on the detector plane

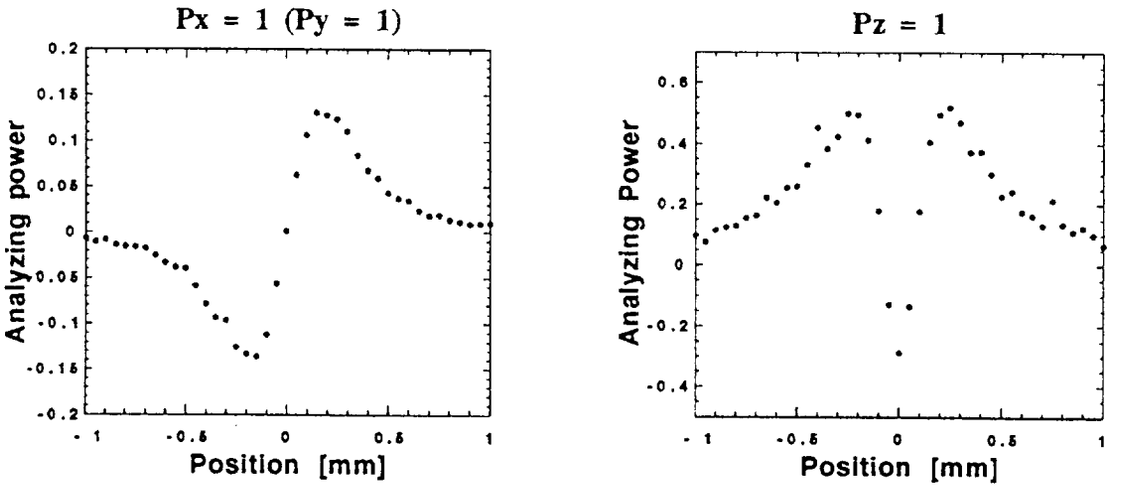

Figure 16: Analyzing power of the asymmetry measurement for scattered γ's on the detector plane

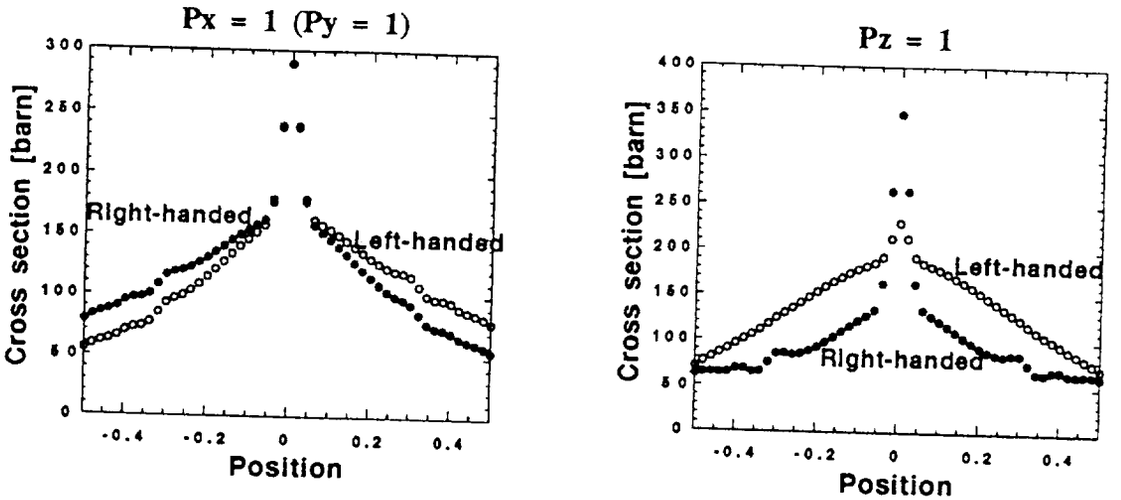

Figure 17: Distribution of scattered e^-'s on the detector plane

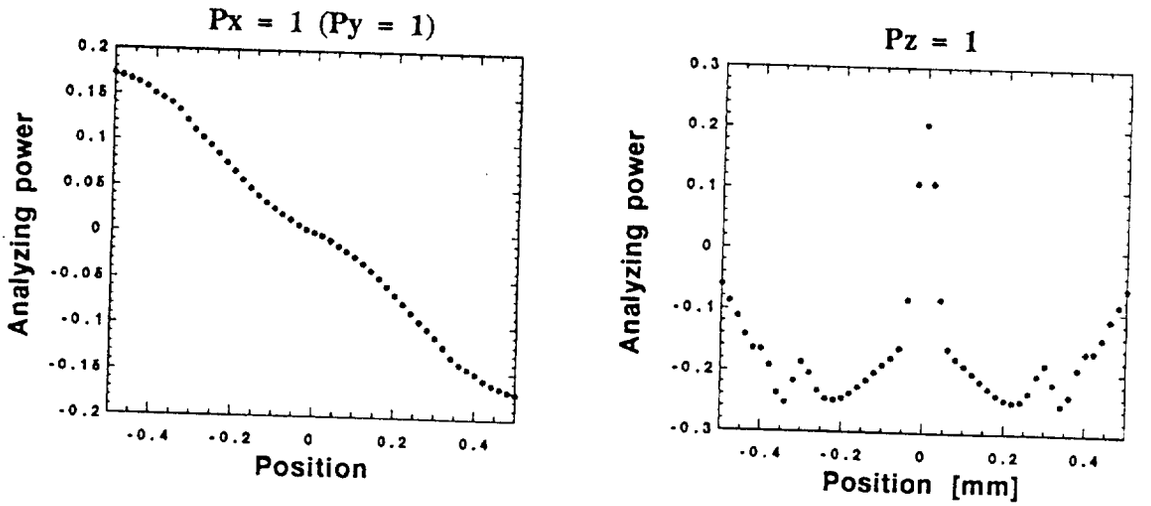

Figure 18: Analyzing power of the asymmetry measurement for scattered e^-'s on the detector plane

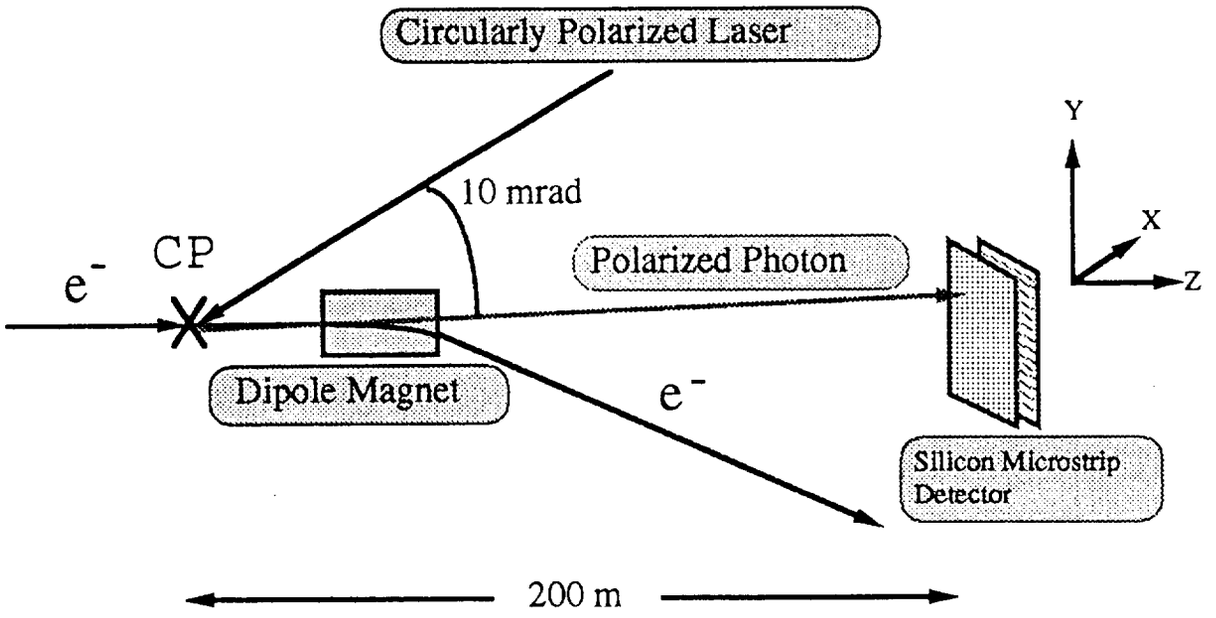

Figure 19: Principle for measuring the arbitrary beam polarization

5 Monte–Carlo simulations for polarization measurements at JLC

5.1 Measurement of scattered photons

We utilize asymmetric distributions of scattered γ's and/or e^-'s. Both scattered γ's and e^-'s are highly collimated into the direction of the primary e^- beam, because the energy of the e^- beam is much larger than that of the laser beam. Therefore, as shown in Fig 14, we need to place dipole magnets at a downstream position from the CP in order to separate the scattered γ's from the e^- beam. However, these dipole magnets produce shynchrotron radiation (SR), thus giving rise to serious background. We will come back to this issue in Sec 5.2. The scattered γ's are measured with a silicon micro–strip detector. A thin target material, where the e^+ and e^- are pair–created, must be located near to the detector. The EGS4 code was utilized to simulate the e^+e^- pair-creations at the target material (tungsten) having a thickness of 1 mm by signal and shynchrotron γ's. The number of pair–created e^-'s and e^+'s are saturated in thicker tungsten. It is assumed that tungsten is located 1 mm upstream from the detector plane.

We simulated the distribution of scattered γ's and the asymmetry on the detector plane under the configuration discussed in Sec 4.2, as shown in Figs 20 and 5.1. The divergence of pair–created e^+ and e^- due to multiple scattering in tungsten is very small, and negligible compared with the resolutions of the position measurement, since the energy

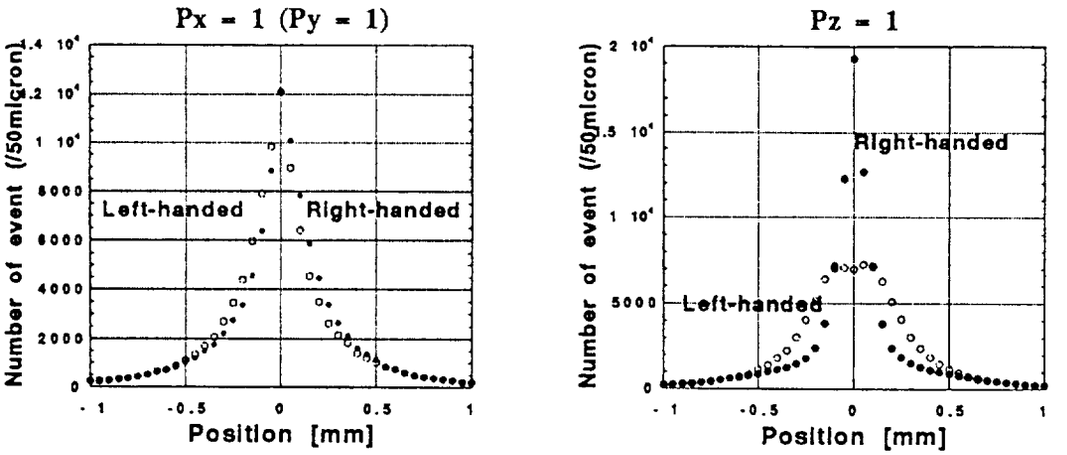

Figure 20: Distribution of Monte-carlo scattered γ's on the detector plane

of the scattered γ's is of GeV order.

In this case, the polarization of the e^- beam measured by Compton scattering is changed from that at the IP, since we locate additional quadrupole magnets to refocus the outgoing e^- beam. Although it is a small effect, the beam polarization at the IP can be restored by calculating the spin precession of the e^-'s.

5.2 Separate signal photons from the background

The luminosity of the laser-e^- interaction with a horizontal crossing angle of δ per one collision is given by

$$L_m = \frac{N_e N_L}{2\pi\sqrt{\sigma_{ey}^2 + \sigma_{Ly}^2}\sqrt{\cos^2(\delta/2)(\sigma_{ex}^2 + \sigma_{Lx}^2) + \sin^2(\delta/2)(\sigma_{ez}^2 + \sigma_{Lz}^2)}}\ , \tag{5.1}$$

where N_e is the number of e^-'s per one bunch, N_L is the number of photon's in one laser pulse and σ_{ex}, σ_{ey}, σ_{ez} (σ_{Lx}, σ_{Ly}, σ_{Lz}) are the rms dimensions of the e^- bunch (the laser pulse). Using another parameter (J(Jule/pulse)) for the intensity and E(eV) for the energy of the laser, N_L is written as

$$N_L = 6.24 \times 10^{18}\frac{J}{E}\ . \tag{5.2}$$

Using the parameters of the laser beam given in Table 4, we calculated $N_L = 1.25 \times 10^{19}$. Assuming that the e^- intensity per bunch is 2×10^{10}, and that the beam sizes of the

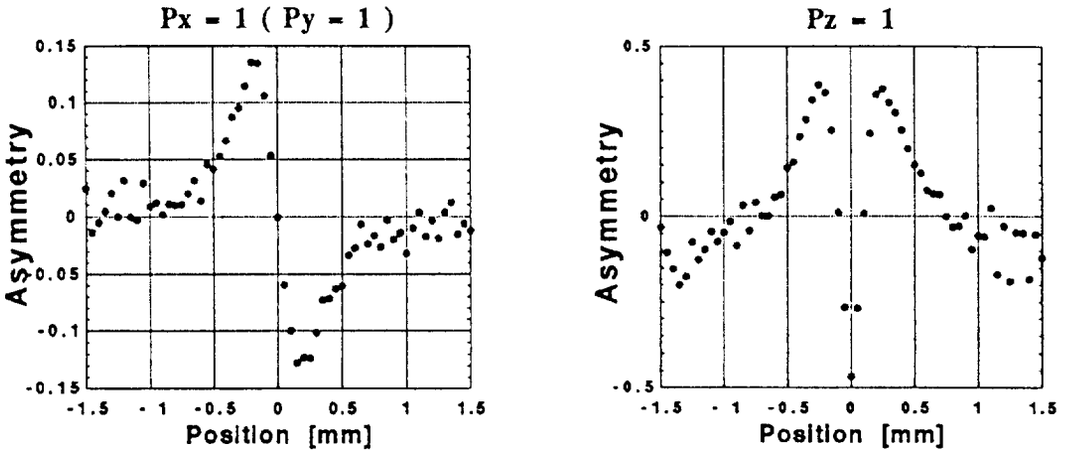

Figure 21: Asymmetry of Monte-carlo scattered γ's on the detector plane

Table 4: Parameters of the laser beam

Wave length	533	nm
Energy	2.33	eV
Diameter	0.5	$mm\phi$
Intensity	1	Jule/pulse
Pulse width	5	ns

Compton-scattered e^- is 20 μm, we obtained a luminosity (L_m) of 2.14×10^{30} cm^{-2}. When the energies of the e^- and laser beams are 250 GeV and 2.33 eV, respectively, the total cross section (σ) is calculated as 135.69×10^{-27} cm^2. Hence, the number of scattered γ's is obtained as

$$N_{signal} = L_m \sigma = 2.90 \times 10^5 \ . \tag{5.3}$$

It is noted that the laser light collides with only one e^- bunch among 100 bunches of 1 pulse, while SR are emitted from each bunch. For a bending angle of the e^- of 1 mrad, the number of SR per 1% band width

$$N_{SR} = 2.68 \times 10^{-9} \gamma_e n N_e G_1 \ , \tag{5.4}$$

where γ_e is the gamma factor of the e^-beam, n is the number of bunches per one pulse,

and G_1 is given by

$$G_1 = \frac{\lambda_c}{\lambda} \int_{\lambda/\lambda}^{\infty} K_{5/3}(\eta) d\eta \ . \tag{5.5}$$

The parameter λ_c represents the critical wavelength, given as

$$\lambda_c(\mathring{A}) = \frac{5.59\rho(m)}{E^3(GeV)} \ , \tag{5.6}$$

where E is the energy of the e^- beam and ρ is the radius of the e^- trajectory in a magnetic field, given as

$$\rho(m) = 3.336 \frac{E(GeV)}{B(T)} \ . \tag{5.7}$$

The critical energy (E_c) was obtained to be

$$E_c(keV) = \frac{2.218E^3(GeV)}{\rho(m)} = 0.665B(T)E^2(GeV) \ . \tag{5.8}$$

Assuming that the magnetic field of the dipole magnets is about 0.5 T, we need to bend the e^- beam only 5 mrad so as to avoid a collision with a detector located 150 m downstream from the dipole magnet. In this case, the critical energy is about 20.8 MeV; thus, less than a half of the SR's will reach the detector plane 200 m downstream. The number of these SR's per band width of 1% is estimated to be

$$N_{SR} \approx 6.0 \times 10^8 G_1 \ , \tag{5.9}$$

giving rise to the total number of the SR to be

$$N_{SR}(TOTAL) = 2.21 \times 10^{11} \ . \tag{5.10}$$

The energy distribution of these SR's is shown in Fig 22. Hence, from Eqs 5.10 and 5.3, the ratio of the signal γ's to the background γ's is estimated to be $S/N \approx 1 \times 10^{-6}$.

Fig 23 shows the horizontal and vertical distributions of $e^{\pm}$ caused by SR. To separate the signal γ's from the background γ's, we propose to provide a distance of 1 m between the tungsten and detector, and to insert two types of magnets so as to suppress pair-created e^+e^- caused by background γ's, corresponding to the horizontal and vertical polarization measurements. For example, a magnetic field of 0.03 T bends $e^{\pm}$ with 200 MeV (100 GeV) outward with a distance of about 20 mm (40 μm) from the center of the detector, as shown in Fig 24. Here, the γ's which have not created e^+e^- pairs in the tungsten, however, directly enter the silicon micro-strip detector. The horizontal and vertical distributions of pair-created e^+e^- from signal γ's on the detector plane and the asymmetry for the right and left handed laser beams are shown in Figs 25 and 26, respectively. Comparing these results with Figs 20 and 5.1, we obtain similar patterns in spite of the large fluctuation in the data due to the small numbers of Monte-Carlo events.

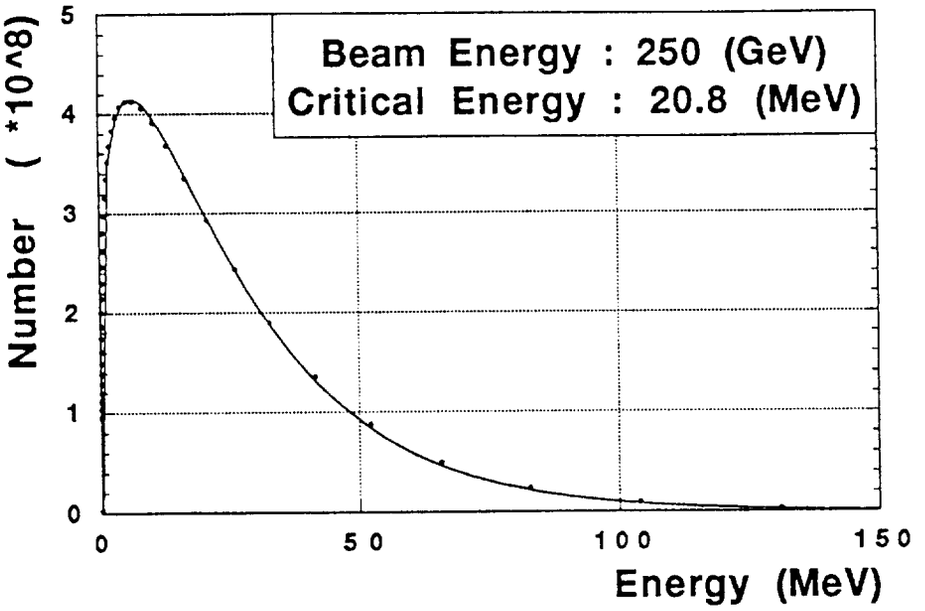

Figure 22: Energy distribution of the γ's emitted by an e^- beam with an energy of 250 GeV when it traverses through the dipole magnets

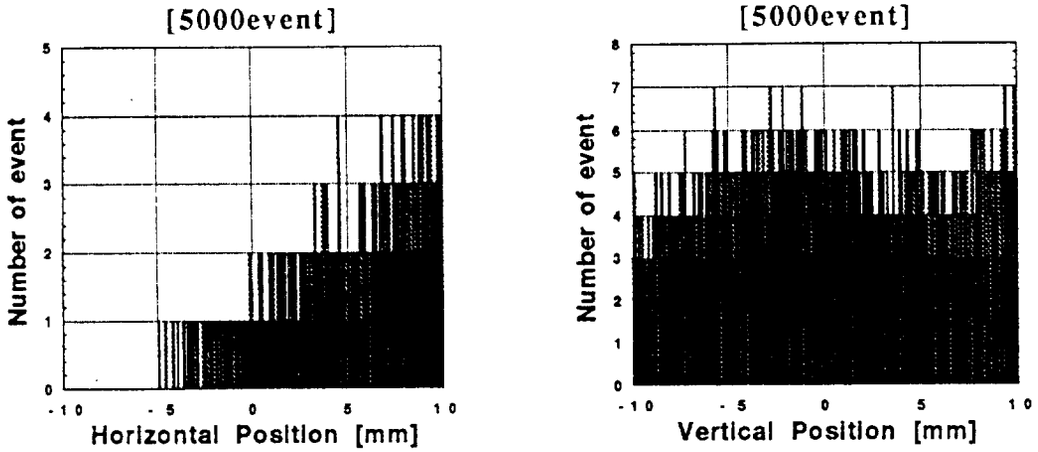

Figure 23: Distribution of the Monte-Carlo background γ's on a detector 1 mm downstream from the tungsten

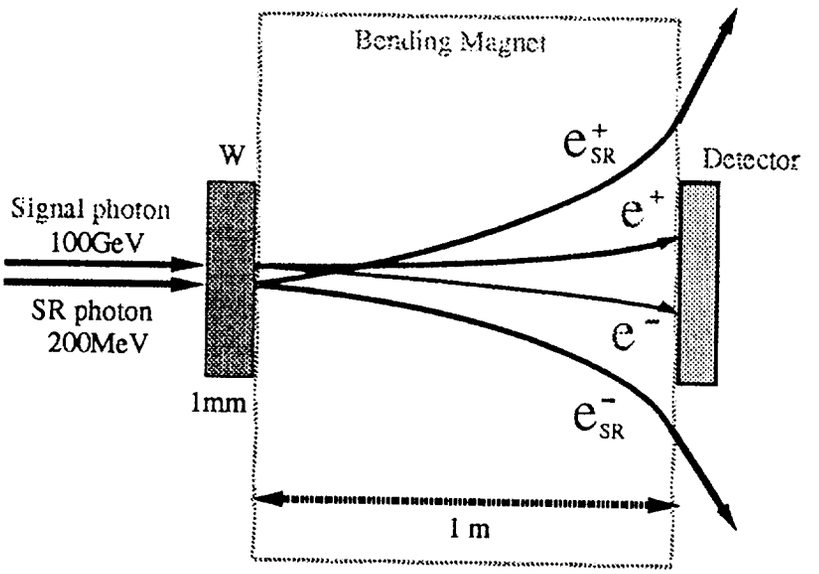

Figure 24: Proposed layout of the detector system

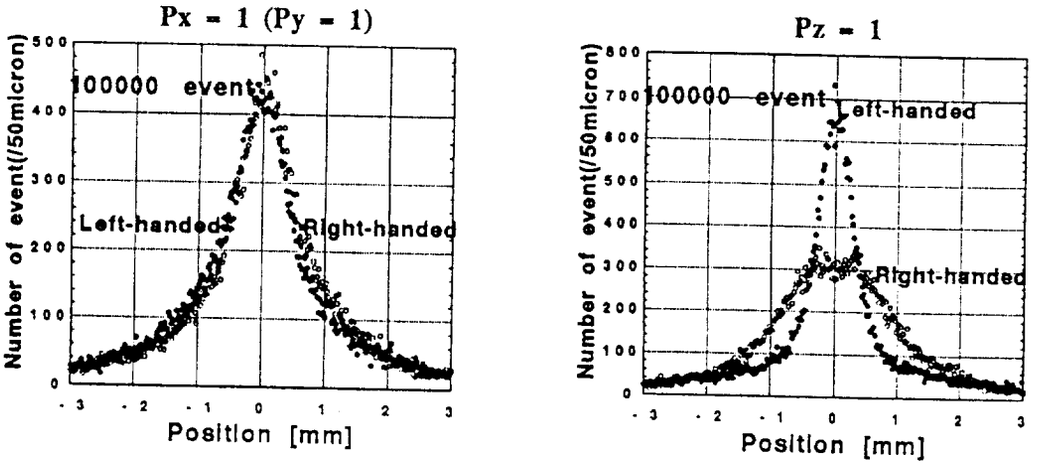

Figure 25: Distribution of the Monte–Carlo scattered γ's on a detector 1 m downstream from the tungsten

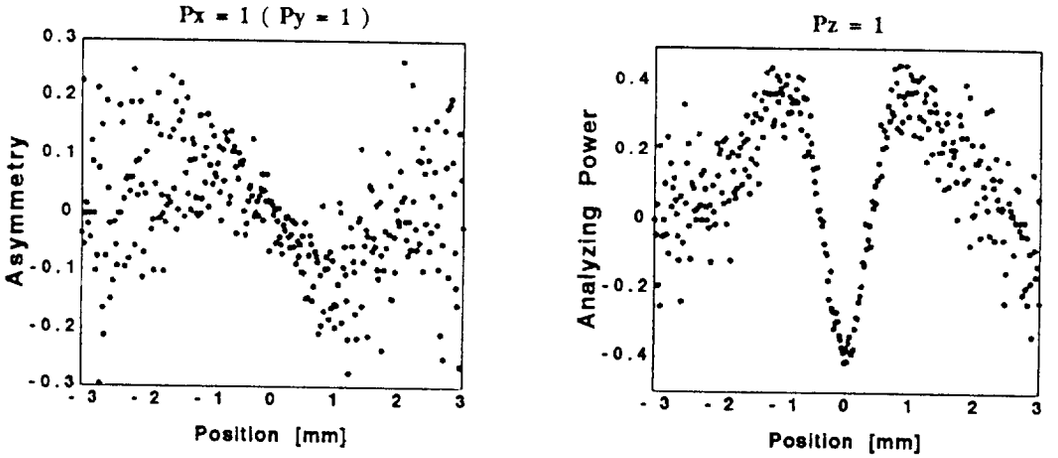

Figure 26: Asymmetry of Monte–Carlo scattered γ's on a detector 1 m downstream from the tungsten

6 Conclusion

In this report, we present a new idea for measuring both the longitudinal and transverse components of $e^{\pm}$ beams in future linear colliders by utilizing the Compton scattering of a laser with $e^{\pm}$ after the IP. Since the $e^{\pm}$ beams have a large angular spread after the interaction, and thus the resolution of a polarization measurement is considerably deteriorated, we propose to refocus the $e^{\pm}$ beams at a point far downstream from the IP (i.e. 200 m) by inserting a quadrupole–magnet between the IP and the collision point of the laser with $e^{\pm}$. If the beam is focussed on the detector plane with a spot size of 20 μm diameter, we can obtain a reasonable magnitude of the analyzing power of about 15% in the transverse direction and 50% in the longitudinal direction.

If we put our proposed method into practical using a polarization measurement, we will meet with the serious problem of background caused by synchrotron radiation, which is generated when the outgoing e^{-} is bent away in the dipole magnet. Actually, the magnitude of the background is 10^6–times larger than that of the signal. To examine realistic conditions of how to extract the signal γ–rays, we performed a detailed Monte–Carlo simulation. One possible method is to utilize the characteristics of the synchrotron radiations that their energies are extremely low, i.e. the maximum energy is only 400 MeV, while the energy of the signal γ–rays is on the order of 100GeV. we thus insert two types of bending magnets between the tungsten target and the detector, and almost completely supress the background.

According to our knowledge obtained in this analysis, we are now carring more realistic studies, particularly a detailed design of the detector system, by improving the Monte-Carlo simulation.

Acknowledgement.

We would like to thank Dr.K.Nakajima and Dr.K.Oide of KEK for fruitful discussions. This research is partially supported by a research fund of KEK for cooperative developments.

References

[1] J . Fleischer and K . Kolodziej, Phys. Rev. D49, 2174 (1994).

[2] K . Hagiwara and D . Zeppenfeld, Nuclear Physics B274(1986)1-32, North-Holland, Amsterdam

[3] F . W . Lipps and H . A .Tolhoek, Physica 20 (1954) 85. ; F . W . Lipps and H . A .Tolhoek, Physica 20 (1954) 395.

[4] K . Fujii and T . Omori, LC physics note, KEK, 17/Jul/1995.

[5] JLC Group, KEK Report 92-16, December 1992.

[6] T . Omori, Proceedings, 3rd JLC Workshop, KEK, 18-20/Feb/1992.

[7] T . Omori, Polarized Positron Beam Group for JLC, meeting paper for details about Polarimeter with Laser-Compton scattering, 28/Dec/91

[8] M . J . Fero, for details about the Compton polarimeter for SLC

[9] E . E . Koch, Handbook on Synchrotron Radiation, Vol. I, p . 65 ., North Holland Publishing Company, 1983